Food Hydrocolloids 172 (2026) 111936

Contents lists available at ScienceDirect

Food Hydrocolloids

journal homepage: www.elsevier.com/locate/foodhyd

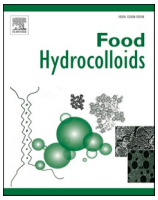

Soluble amylose chains inhibit gelatinisation and retrogradation in waxy corn starch

Thoithoi Tongbram [a,b], Lathika Vaniyan [a], Thomas MacCalman [c], Avanish Bharati [d], Frederick J. Warren [e], Laxmikant Shivnath Badwaik [b], Pallab Kumar Borah [a,f,*], Gleb E. Yakubov [a,g,**]

[a] Food Materials Research Group, School of Biosciences, University of Nottingham, Sutton Bonington, LE12 5RD, United Kingdom
[b] Department of Food Engineering and Technology, School of Engineering, Tezpur University, Napaam, 784028, India
[c] National Centre for Macromolecular Hydrodynamics, School of Biosciences, University of Nottingham, Sutton Bonington, LE12 5RD, United Kingdom
[d] Jülich Centre for Neutron Science, Forschungszentrum Jülich GmbH, Lichtenbergstraße 1, 85747, Germany
[e] Quadram Institute Bioscience, Norwich Research Park, Norwich, NR4 7UQ, United Kingdom
[f] Heinz Maier-Leibnitz Zentrum, Technical University of Munich, Lichtenbergstraße 1, 85748, Germany
[g] School of Food Science and Nutrition, University of Leeds, Leeds, LS2 9JT, United Kingdom

ARTICLE INFO

Keywords:
Waxy corn starch
Soluble amylose chain
Amylopectin
Isoamylase debranching
Gelatinisation
Retrogradation

ABSTRACT

In this study, soluble amylose chains with varying degrees of polymerisation (DP 186–4020) were isolated via isoamylase debranching of amylopectin from native and waxy corn starches. When these soluble amylose chains are mixed with aqueous suspensions of waxy corn starch, spontaneous adsorption onto the surface of starch granules occurs. The resulting coating envelops the granules and markedly inhibits gelatinisation, increasing the onset temperature by up to 10 °C. Additionally, the amylose coating alters the pasting and short-term retrogradation properties of waxy corn starch, as evidenced by a reduction in trough viscosity, up to a 20 % decrease in breakdown viscosity, and approximately a 50 % increase in setback viscosity. This effect is both concentration- and DP-dependent. We found that chains with a critical length of $200 \leq DP \leq 700$ produce the most pronounced effect and exhibit the strongest concentration dependence, suggesting that entropic considerations play a key role in starch–amylose interactions. Complementary analyses – including calorimetry, viscosity, turbidity measurements, and small-angle X-ray scattering – confirmed the inhibited gelatinisation and retrogradation. X-ray diffraction data further corroborated that the adsorbed amylose forms a hydrated, V-type-like polymorphic envelope. We hypothesise that this amylose coating restricts water ingress and inhibits granular gelatinisation, providing a physical basis for the observed inhibition. These findings highlight a previously undocumented role of soluble amylose chain length in directing starch thermal and structural transitions. Our results advance the fundamental understanding of starch–amylose interactions and offer a novel route for designing starch systems with enhanced functionality for applications in food processing and, more broadly, in (bio)material design.

1. Introduction

Starch is one of the most abundant hydrocolloids in nature and is considered an ideal material due to its non-toxicity, global availability, hydrophilicity, and biodegradability. It is also one of the most important polysaccharides used in the food industry for a variety of applications, such as thickening, gelling, viscosity modulation, and improving the texture and stability of food products (Chen et al., 2024, 2025; Cui et al., 2018; Ma et al., 2019; Zhan et al., 2025). However, the suitability of native starch may be limited due to its instability under heat and shear, sensitivity to acidic conditions, and its tendency to impart undesirable qualities to food products upon cooling (Zhou et al., 2017), such as a stale taste in baked goods or syneresis in condiments and jellies. The unique techno-functional properties of starch are underpinned by two key structural transitions: gelatinisation and retrogradation. In the presence of moisture and upon heating, starch undergoes a complex structural transformation involving water absorption, granule swelling and expansion, destabilisation, and the eventual collapse of its native ordered structure – an irreversible structural transition known as

* Corresponding author. Food Materials Research Group, School of Biosciences, University of Nottingham, Sutton Bonington, LE12 5RD, United Kingdom. .
** Corresponding author. Food Materials Research Group, School of Biosciences, University of Nottingham, Sutton Bonington, LE12 5RD, United Kingdom. .
E-mail address: g.yakubov@leeds.ac.uk (G.E. Yakubov).

https://doi.org/10.1016/j.foodhyd.2025.111936
Received 14 July 2025; Received in revised form 3 September 2025; Accepted 4 September 2025
Available online 9 September 2025

Glossary

DP	degree of polymerisation
SEC-MALS	Size exclusion chromatography coupled to multiangle light scattering
5-DTAF	5-(4,6-dichlorotriazinyl) aminofluorescein
M_w	Weight average molar mass
MWCO	molecular weight cut-off
K_B	Boltzmann constant
ζ_0	monomer friction
ζ	total chain friction
η_s	solvent viscosity
cP	centipoise
Pa.s	Pascal-second
AP	waxy corn starch

gelatinisation (Donovan, 1979; Ratnayake & Jackson, 2007; Waigh et al., 2000). Upon cooling, gelatinised starch undergoes a reverse structural transition known as retrogradation, which is undesirable in many food processing and food technology applications.

Starches are composed of *d*-glucose monomer units joint together by (1 → 4)-*α* linear and (1 → 6)-α branching linkages (Junejo et al., 2022; Whelan, 1971). Depending on the type of linkages, starches can be distinguished into two homopolymer forms, *i.e.*, amylose with a linear backbone and highly branched amylopectin (Pérez & Bertoft, 2010). The amylose and amylopectin chains hierarchically pack in alternating layers of amorphous and semi-crystalline domains within starch granules (Jenkins & Donald, 1998; Pérez & Bertoft, 2010; Waigh et al., 1998). The significance of this structural feature is in its impact on starch structural transformation upon heating and cooling. During retrogradation, disassembled chains of amylose and amylopectin present in gelatinised starch reassociate to form ordered structures (Wang et al., 2015). However, the structural order of retrograded starch is markedly different from its native structure, making the hysteresis between gelatinisation and retrogradation irreversible. Tailoring starch gelatinisation and retrogradation is therefore essential for achieving precise control over its techno-functional properties and, consequently, for modulating the physicochemical characteristics of starch-based products.

To overcome the well-documented drawbacks of native starch gelatinisation and retrogradation, polyols, mono-, di-, and oligosaccharides (e.g., sucrose), as well as non-starch hydrocolloids, are often used in combination or blends with native starch (Chen et al., 2014). By modulating starch gelatinisation and retrogradation, these additives help improve heat and shear stability and can maintain or modify the overall quality of starch during food processing and storage by altering its rheological properties and textural attributes (Zhou et al., 2017). Sugars are long known to increase gelatinisation temperature (Perry & Donald, 2002), and affect the gelatinisation enthalpy, swelling, and pasting behaviour of starch, and a comprehensive review has been provided by BeMiller (BeMiller, 2011). For example, saccharides such as ribose, fructose, glucose, sucrose, lactose, trehalose, maltose, raffinose, and stachyose have been shown previously to protect starch crystalline structure during gelatinisation (Li et al., 2015). Disaccharides such as trehalose, sucrose, lactose, and maltose have also been shown to retard the gelatinisation of corn starch (Li et al., 2015). Oligosaccharides such as low molecular weight dextrin, inulin, soluble fibres such as oligofructoses, and non-starch polysaccharides like pullulan, pectin, konjac glucomannan, and xanthan gum are also known to delay the gelatinisation of starch, including reduction of peak viscosity during gelatinisation process (Chen et al., 2019, 2022; Durán et al., 2001; Fu et al., 2025; Gao et al., 2025; Luo et al., 2017; Renzetti et al., 2021; Sheng et al., 2018; Ye et al., 2024; Zhao et al., 2024). Several theories have been proposed to explain the effects of sugar and hydrocolloid additives on the gelatinisation and retrogradation of starch. One perspective suggests that sugars and similar oligomers migrate into the interior of starch granules during starch gelatinisation and increase carbohydrate chain-chain interactions, thereby hindering gelatinisation and swelling of starch granules, and increasing gelatinisation temperature (Chen et al., 2022; Li et al., 2015; Pourmohammadi et al., 2018). Another theory suggests that the presence of sugars and oligomers reduces the available water, disrupting the interaction between starch chains and water molecules necessary for gelatinisation (Kohyama & Nishinari, 1991). Studies have linked the number of hydroxyl groups in polyols (e.g., glycerol), sugars, and oligomer additives to the co-solute-induced changes in starch gelatinisation. Although these compounds effectively form H-bonds with starch, they are considerably less effective plasticizers than water (Baek et al., 2004; Pourmohammadi et al., 2018). Thus, the extensive body of literature provides comprehensive insights on the effect of polyols, sugars, and oligosaccharides on starch gelatinisation. However, these effects become much less documented if a broader range of degree of polymerisation (DP) is considered, which may restrict the generalisability of the findings.

Building on this background, we isolated soluble amylose chains *via* isoamylase debranching of amylopectin present in native and waxy corn starch granules, yielding chains with DP ranging from 186 to 4020, characterised using size exclusion chromatography-multi angle light scattering (SEC-MALS). To enable probing the lower end of the DP spectrum and aid comparison with previous works, we additionally included maltose (DP 2) and maltodextrin (DP_{avg} 20) in our sample set. We hypothesized that incorporating soluble amylose chains would lead to marked alterations in starch gelatinisation and retrogradation behaviour. Complementary characterisation was carried out using calorimetry, viscosity and turbidity analyses, microscopy (polarised and fluorescence), small-angle X-ray scattering and wide-angle X-ray diffraction. A method to synthesise fluorophore-attached soluble amylose chains is also described, which found use in our fluorescence imaging study and may find further use in polymer tracking studies.

Results from our study are expected to provide promising avenues to tune gelatinisation and retard retrogradation of starch granules, which is useful in industrial processes where premature thickening, early recrystallisation, staling, and syneresis are undesirable. These insights will also guide the rational design of starch-based slow digestible functional foods and stimulate development of advanced biomaterials for 3D printing, edible coating, and pharmaceuticals.

2. Materials and methods

2.1. Materials

Waxy corn starch (ca. 99 % amylopectin, Amioca powder TF-04400108) and isoamylase enzyme ($\geq 10^7$ units mg^{-1} protein) were purchased from Ingredion Inc., USA and Megazyme, Ireland, respectively. Native corn starch (~75 % amylopectin), maltose, maltodextrin (degree of esterification, 4–7; degree of polymerisation, 14–25), and 5-DTAF (5-(4,6-dichlorotriazinyl) aminofluorescein) were purchased from Sigma Aldrich, UK. All chemicals were of analytical grade, unless stated otherwise. Milli-Q water (18.2 MΩ cm ionic purity at 25 °C) purified using a Milli-Q apparatus (Millipore Corp., USA) was used throughout the experiments.

2.2. Isolation of soluble amylose chains

Soluble amylose chains were isolated from both waxy and native corn starch using isoamylase hydrolysis (40 °C, pH 4.0, 24 h), as described earlier but with minor modifications (Ciric et al., 2014; Jung et al., 2022). Briefly, 100 mg of starch was dispersed in 10 mL of sodium acetate buffer at pH 4 and heated to 95 °C for 15 min to induce gelation. Following gelation, starches were cooled to 40 °C. 6 μL of isoamylase

($\geq 10^7$ units mg^{-1} protein) was added to the resultant cooled 1 % (w/v) starch gel, homogenised on an Ultra Turrex T24 (IKA Labotecnik, Germany) (8000 rpm for 1 min at 25 °C), and incubated at 40 °C for 24 h under continuous stirring. The mixture was then heated to 95 °C to cease the reaction, cooled to 25 °C, centrifuged at 4000g for 2 min, and the supernatant was collected. Following centrifugation, the pellet was dissolved in pre-warmed sodium acetate buffer (pH 4) at 35 °C, centrifuged at 4000g for 2 min, and the second supernatant phase was collected. Both supernatants were snap frozen in an ethanol ice bath and then lyophilised. Throughout the rest of the manuscript, the resulting fractions were termed as soluble amylose chains and were referred to as W/N for the waxy/native sources followed by an index 25 or 35 to reflect the extraction temperature (°C). Note, we verified that these fractions are without any traces of residual isoamylase by monitoring the UV–Vis absorbance for protein at 280 nm (Supplementary Information, Fig. S1).

Weight average molar mass (M_w) and polydispersity of soluble amylose chains, *i.e.*, 25W and 35W, and 25N and 35N were estimated using size exclusion chromatography coupled to multi-angle light scattering (SEC-MALS, Wyatt Technology, USA), as described elsewhere (Chun et al., 2020). Briefly, samples (1 mg mL^{-1}) were injected in the SEC portion consisting of a Postnova Analysis PN7505 degassing unit, a Shimadzu LC-10 AD HPLC pump, a Spark-Holland Marathon Basic autosampler, and a Shodex™ LB-805 column equipped with a Shodex™ LB-G6B guard column connected in series. The SEC portion was coupled in-line to a Dawn® Heleos™-II MALS (Wyatt Technology, USA) light scattering photometer and an Optilab® rEX refractive index detector to measure MALS intensities simultaneously at 18 angles as a function of elution volume. A 4 mW He-Ne laser was used at a wavelength of 658.6 nm, and the refractive increment for all samples was taken as 0.1510 mL g^{-1} and RI was 1.331. Samples were filtered using Whatman® Puradisc 25 syringe filters, 0.2 μm, PVDF and a 50 μL aliquot of each solution was injected onto the columns at room temperature. The eluent employed was phosphate buffer (0.1M, pH 7) at a flow rate of 0.5 mL min^{-1}. ASTRA™ (version 6) software was used to calculate the weight-average molecular weight (M_w) and polydispersity ($M_w\ M_n^{-1}$).

2.3. Preparation of waxy corn starch - soluble amylose chain systems and thermal analysis

Soluble amylose chains were incorporated into waxy corn starch dispersions by simple mixing. Briefly, waxy corn starch was mixed with soluble amylose chains to achieve a biopolymer ratio of 1:0, 1:0.25, 1:0.50, 1:0.75, and 1:1 (waxy corn starch: soluble amylose chains, w/w). The water content in the systems were varied from 50 to 75 % (w/w) to ensure mass balance (moisture equilibration time ~ 12 h) and are shown in detail in Table 1. Pure waxy corn starch was used as control, and maltose or maltodextrin was added in the same ratios to waxy corn starch instead of soluble amylose chains which served as comparators. Differential scanning calorimetry was performed on a DSC3+ calorimeter (Mettler-Toledo, UK) using sealed aluminium pans in the temperature range of 20–95 °C at a scan rate of 10 °C min^{-1}.

Table 1
Biopolymer ratio and water content in waxy corn starch-soluble amylose chain mixtures.

Biopolymer ratio	Waxy corn starch	Soluble amylose chain	Water	Total	Water Content
		(parts)			(%)
1:0	1	0.00	3.00	4.00	75.00
1:0.25	1	0.25	2.75	4.00	68.75
1:0.50	1	0.50	2.50	4.00	62.50
1:75	1	0.75	2.25	4.00	56.25
1:1	1	1.00	2.00	4.00	50.00

2.4. Pasting properties

Changes in pasting properties were monitored in a Perten RVA 4800 (PerkinElmer, USA). The starch samples were hydrated at 90–95 % (w/w) water content, and then homogenised using an Ultra-Turrax T18 high-speed homogenizer (IKA, Germany) at 8000 rpm for 1 min at 25 °C. The pasting profile followed: heating to 50 °C and then holding for 1 min, heating to 95 °C within 3 min 40 s and holding at 95 °C for 2 min 30 s, cooled to 50 °C within 3 min 40 s and hold at 50 °C for 1 min 30 s. Rotor speed of 160 rpm was maintained during the entire profile.

2.5. Turbidity analysis

Turbidity was analysed using a Crystal16® system (Technobis Crystallization Systems, Netherlands), equipped with 16 reactors with bottom mounted stirrers. The water content in the starch samples was varied from 98 to 99 % (w/w). Samples were heated from 25 °C to 95 °C at a rate of 1 °C min^{-1} alongside stirring at 200 rpm, held at 95 °C for 30 min with stirring at 200 rpm, and then cooled to 25 °C at 1 °C min^{-1} without stirring. Log of transmittance (%) and temperature (°C) were plotted as a function of time (min) to study the turbidity profile. Milli-Q water was used as control.

2.6. Fluorescence microscopy

Soluble amylose chains were fluorescently labelled with 5-DTAF (5-(4,6-dichlorotriazinyl) aminofluorescein), as described previously but with minor modifications (Alshammari et al., 2024; Khin et al., 2021). Briefly, 0.2 mM 5-DTAF was added to 10 mg mL^{-1} soluble amylose chains and gradually mixed with 10 mM Na_2SO_4 over 2 min. To initiate the reaction, pH was raised to 10 using 10 % NaOH (w/v, 2.5M) in the dark for 2 h. Two volumes of ethanol/sodium acetate buffer mixture (1:2 ratio of 0.055 M sodium acetate (pH 5.4) to ethanol) was added to quench the reaction. Unbound 5-DTAF was removed with sodium acetate: ethanol solution using ultracentrifugation in Sartorious Vivaspin® Ultra centrifugal dialysis filter (MWCO, 3 kDa) until the filtrate was clear of 5-DTAF (absorbance of filtrate was monitored until the filtrate reaching constant values, 492 nm). Fluorescently labelled soluble amylose chains were then progressively dehydrated with increasing concentrations of ethanol (wash1: 50 % ethanol, wash2: 80 % ethanol, wash3: 99 % ethanol) before a final wash with acetone. 5-DTAF-soluble amylose chains was redissolved in water and then freeze dried. Freeze dried 5-DTAF-soluble amylose chains were mixed with waxy corn starch and then heated till 95 °C. Upon cooling, gels were deposited on an observation slide and visualised using an AMG EVOS® FL fluorescent microscope (ThermoFisher Scientific, USA). Soluble amylose chains were additionally mixed with waxy corn starch granules and then imaged at 25 °C on an Eclipse E400 fluorescence microscope (Nikon, Japan). λ_{ex}, 470 nm and λ_{em}, 525 nm.

Loss of birefringence in samples was monitored in the temperature range of 25 → 95 °C using a polarised light microscope equipped with a high-resolution digital camera and a Linkam THMS600 stage coupled to a Linkam T96 temperature controller (Linkam Scientific, UK). The heating rate was 2 °C min^{-1}.

2.7. Small-angle X-ray scattering and wide-angle X-ray diffraction

Small-angle X-ray scattering (SAXS) experiments were performed on the Garching KWS-X XENOCS XUESS 3.0 XL beamline equipped with a high-flux metal jet source (Excillum D2+) operated at 70 kV and 3.57 mA. The sample-to-detector (Eiger 2R 4M detector) distance was 0.65 m. Temperature-dependent measurements were carried out in 2 mm sealed capillaries on a temperature-controlled Peltier stage at steady-state (20–90 °C, heating rate, 2 °C min^{-1}). Silver behenate with a known lattice spacing of 5.84 nm was used to calibrate the scattering vector q as, $q = 4\pi/_{\lambda} \sin\theta$, where λ, 0.1314 nm (Ga-Kα radiation) and 2θ is the

scattering angle. The 2D patterns were normalised to an absolute scale and azimuthally averaged to obtain the 1D intensity profiles, followed by the subtraction of the empty cell background. A scaling of 0.955 was utilised to account for water contribution at high-q. The parameters of the lamellar structure from SAXS ($0.1\ nm^{-1} < q < 1.5\ nm^{-1}$) were obtained by least square fitting employing the Levenberg-Marquardt optimisation algorithm to a Cauchy-Lorentz-Power Law equation (Borah et al., 2019a) as, $I(q) = I_{max}\left[1 + \left(\frac{(q-q_{max})}{\Delta q}\right)^2\right]^{-1} + Aq^{-\delta}$ in OriginPro 2025, where I_{max}, q_{max}, Δq, A, and δ are positive adjustable parameters. The half width at half maximum (HWHM), Δq, in reciprocal space, was converted to real space to calculate the average lamellar thickness variations as, $HWHM\ (real\ space) = \frac{\pi\Delta q}{q_{max}{}^2 - \Delta q^2}$.

Wide-angle X-ray diffraction (XRD) data were recorded in the 2θ range of 5–30° in the temperature range of 20–90 °C (heating rate, 2 °C min^{-1}) using an Echo D8 Advance Bruker AXS powder diffractometer (Bruker, UK). The setup used in this study has been described in our previous report (Vaniyan et al., 2025). The spectra were baseline corrected and relative crystallinity (X_c, %) was calculated as, $X_c = \frac{\sum_{i=1}^{n} A_{ci}}{A_t}$, where A_{ci} is the area under each crystalline peak with index i; and A_t is the total area of the diffraction pattern. Note that the XRD spectra are reported using both the 2θ scale and the q scale, defined as $= \left(4\pi/\lambda\right) sin\, 2\theta/2$, to aid comparison with the SAXS data. Crystallographic information files (CIF) for A-amylose and poly (amylose) potassium hydroxide trihydrate are from the CCDC database (https://www.ccdc.cam.ac.uk/) and the powder XRD patterns were simulated in VESTA (https://jp-minerals.org/vesta/en/).

3. Results and discussion

3.1. Isoamylase debranching of waxy and native corn starch

We utilised isoamylase for isolating the soluble amylose chain as the enzyme specifically cleaves α-1,6-glucosidic linkages at branch points of amylopectin. Since amylopectin is known to have a polymodal distribution of chain lengths (Hizukuri, 1986), we expected isoamylase debranched soluble amylose chains to have a wide range of degree of polymerisation (DP). Soluble amylose chains were isolated from both waxy and native corn starch varieties, and fractions were collected at various temperatures. Our results showed that waxy and native corn starch produced significantly higher yield of soluble amylose chains at 25 °C than at 35 °C, yield ca. 85 % and 10 %, respectively (w/w). Beyond 35 °C, fractions were collected until 95 °C with 10 °C increments of buffer temperature from waxy and native corn starch. However, the yield of the further six fractions were negligible and are not discussed further in this study. Details of yields are provided in Supplementary Information, Table S1.

We determined the molecular weight (M_w), polydispersity index, and DP of all four soluble amylose chain fractions, *i.e.*, termed as 25N, 35N, 25W, and 35W using SEC-MALS (Table 2). The M_w and polydispersity index of soluble amylose chains were found to be in the range of 3.01×10^4 - 6.52×10^5 g mol^{-1} and 2.7–4.8, respectively, and are shown in Table 2. The average molecular weight of amylose is known to be in the order of 1–5 $\times 10^5$ g mol^{-1} (Ai & Jane, 2016), therefore in this study, we classify the soluble amylose chains with $M_w \approx 10^4$ as short-soluble amylose chains, and $M_w \approx 10^5$ as long-soluble amylose chains. Our results are in close agreement with existing literature, where a broad polydispersity for amylose is usually reported, typically between 1.3 and 10 (Le-Bail et al., 2018).

Upon examining the SEC-MALS data for 25W, 35W, and 35N, we observed a bimodal distribution, and the average DP values were calculated to be 704, 216, and 186, respectively. The 25N polymer displayed monomodal distribution with a DP of 4020 (Supplementary Information Fig. S2). Our results for the bimodal distribution of chains agrees with previous reports (Ciric et al., 2014; Li et al., 2020). Soluble amylose chains were completely water soluble (note, turbidity analysis showed transmittance %, ca. 100, data not shown).

Table 2
Physical properties of the soluble amylose chains isolated using isoamylase debranching.

Soluble amylose chains	M_w	Polydispersity	DP
	g mol^{-1}	M_w M_n^{-1}	
25W	1.14×10^5	3.113	704*
25N	6.52×10^5	2.727	4020
35W	3.50×10^4	4.77	216*
35N	3.01×10^4	4.847	186*
Maltose	ND	ND	2
Maltodextrin	ND	ND	~20

Size exclusion chromatography coupled to multi angle laser light scattering (SEC-MALS) was used to estimate the M_w, molecular weight, polydispersity index, and degree of polymerisation (DP). 25W and 35W: soluble amylose chains extracted at 25 °C and 35 °C, 'W' indicates waxy corn starch source; 25N and 35N: soluble amylose chains extracted at 25 °C and 35 °C. N indicates native corn starch source. * Indicates short-soluble amylose chains marked by DP < 1000. ND, not detected.

3.2. Effects of soluble amylose chains on the thermal properties of waxy corn starch

Gelatinisation enthalpy and onset temperatures are two key thermal parameters that determines the extent of gelatinisation. Accordingly, we probed how adding soluble amylose chains to waxy corn starch affects its thermal parameters during gelatinisation, using differential scanning calorimetry. All waxy corn starch-soluble amylose chain mixtures showed starch endothermic transitions with distinct enthalpy and onset temperature, and are shown in Fig. 1A, B and Supplementary Information Table S2. For pure waxy corn starch, no effect on the onset temperature was observed, and our results are in agreement with previous studies (S. Wang, et al., 2016). In these samples, the enthalpy changed from 2.91 ± 0.25 to 5.44 ± 0.09 J g^{-1} for the WMS control samples between 25 % and 50 %, respectively. The onset temperature was observed to be ca. 63 °C for all waxy corn starches, irrespective of solid content. Upon addition of the short-soluble amylose chains, *i.e.*, DP ≤ 1000, we observed an increase in enthalpy accompanied by increase of onset gelatinisation temperature (Fig. 1A, B). Briefly, in waxy corn starch-soluble amylose chains (DP 186, *i.e.*, 35N), we observed an increase in enthalpy from 2.91 ± 0.25 to 7.95 ± 0.38 J g^{-1}, with increase in short-soluble amylose chain addition. Similarly, for waxy corn starch-soluble amylose chain (DP 216 and 704, *i.e.*, 35W and 25W, respectively), enthalpy showed a similar increased from 2.91 ± 0.25 to 6.42 ± 0.62 J g^{-1} and 2.91 ± 0.25 to 7.22 ± 0.59 J g^{-1}, respectively, with an increase in short-soluble amylose chain addition. These enthalpic transitions were accompanied by ca. 10 °C delay in gelatinisation onset temperature (Fig. 1B). Our results closely corroborate previous reports, where incorporation of amylose chains with DP ca. 300 in starch lead to higher onset gelatinisation temperature (Li & Hu, 2021). Luo and coworkers (Luo et al., 2017) also demonstrated that increased addition of inulin (DP, 10–60), a water-soluble linear-chain dietary fibre, increased the gelatinisation onset temperature of wheat starch. However, for waxy corn starch-soluble amylose chain (DP 4020 *i.e.*, 25N), we did not observe any marked changes in enthalpy (enthalpy, 2.91 ± 0.25–3.52 ± 0.24 J g^{-1}), and the thermal transitions were relatively similar to pure waxy corn starch. A delay in onset gelatinisation temperature was still apparent, ca. 10 °C. It appears that the effect of short-soluble amylose chains with DP ≤ 1000 is more pronounced on enthalpy change and onset gelatinisation temperature of waxy corn starch, compared to that of long-soluble amylose chains, *i.e.*, DP ≥ 1000 counterparts.

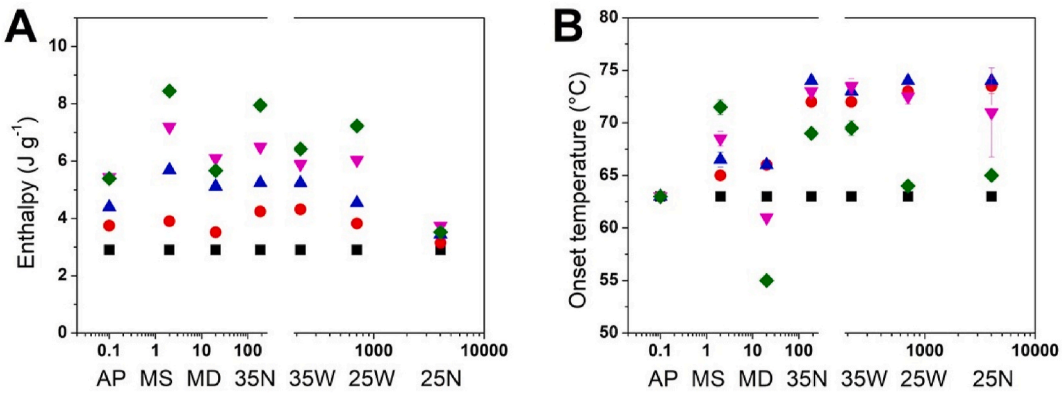

Fig. 1. Effects of soluble amylose chains on the thermal properties of waxy corn starch. Enthalpy as a function of degree of polymerisation, DP of soluble amylose chain (A) and onset gelatinisation temperature as a function of degree of polymerisation, DP of soluble amylose chain (B). Waxy corn starch: soluble amylose chain ratio, 1:0 (■), 1:0.25 (●), 1:0.50 (▲), 1:0.75 (▼) and 1:1 (◆). For total mass balance, 75 %, 68.75 %, 62.5 %, 56.25 %, and 50 % (w/w) water was added, respectively. AP along the x-axis denotes waxy corn starch sample and is plotted for comparison and does not indicate a DP of ~0.1. MS, maltose (DP 2); MD, maltodextrin (DP 20); 35N (DP 186); 35W (DP 216); 25W (DP 704); 25N (DP 4020). In soluble amylose chains (35N, 35W, 25W, and 25N), 25 and 35 refer to the temperature in °C at which the fractions are collected, whereas N and W refer to the origin of these fractions, either native or waxy corn starch varieties. Standard deviations ($n = 3$).

To uncover the effect of soluble amylose chain DP in altering the gelatinisation of waxy corn starch, we used maltose and maltodextrin as comparators. DP of maltose is 2 and of maltodextrin is ca. 20 and provided us with the opportunity to examine these mixed systems in the broad DP range of 2–4020. For all waxy corn starch-maltose systems, changes in enthalpy and onset temperature were markedly greater compared to maltodextrin (Fig. 1A and B). In both mixed systems, increase in maltose and maltodextrin led to an increase in gelatinisation enthalpy and onset temperature. In waxy corn starch-maltose systems, enthalpy increased from 2.91 ± 0.25 to 8.44 ± 0.48 J g^{-1} and onset gelatinisation temperature increased from 63 ± 0.12 to 71.5 ± 0.71 °C, while enthalpy and onset temperature varied from 2.91 ± 0.25 to 5.66 ± 1.22 J g^{-1} and 55 ± 0.36 to 63 ± 0.32 °C, respectively, in waxy corn starch-maltodextrin systems. Our results are concurrent with literature which showed that addition of maltose increases the gelatinisation enthalpy of wheat, potato, and corn starch, and retrograded native and waxy corn starch (Allan et al., 2020; Baek et al., 2004; Li et al., 2015; L. Wang, Xu, et al., 2016), whereas addition of branched limit dextrin and maltodextrin decreases the gelatinisation enthalpy of native and waxy corn, wheat, and cassava starches (Pourmohammadi et al., 2018; Wang et al., 2018).

Polarised-light microscopy further confirmed our findings from calorimetry. Fig. 2A, D shows clear birefringence in waxy corn starch and waxy corn starch-soluble amylose chain granule at 25 °C. A typical Maltese cross pattern is evident arising from the semi-crystalline nature of the starch granules consisting of dense packing of amylopectin chains with a high degree of molecular orientation (Borah et al., 2017; Shi et al., 2021). Loss of birefringence is therefore a key indicator of loss in the ordered structure of starch granules during gelatinisation. As seen from Fig. 2B, waxy corn starch granules undergo complete gelatinisation at 70 °C, and only ca. 2 % granules retain birefringence. However, in the waxy corn starch-soluble amylose chain mixtures, ca. 24 % of the granules continued to exhibit birefringence after being heated to 70 °C (Fig. 2E). This observation constitutes a 10-fold increase in the number of starch granules highlighting delayed gelatinisation. Note, at 90 °C, all systems completely gelatinise (Fig. 2C–F) and is concurrent with our

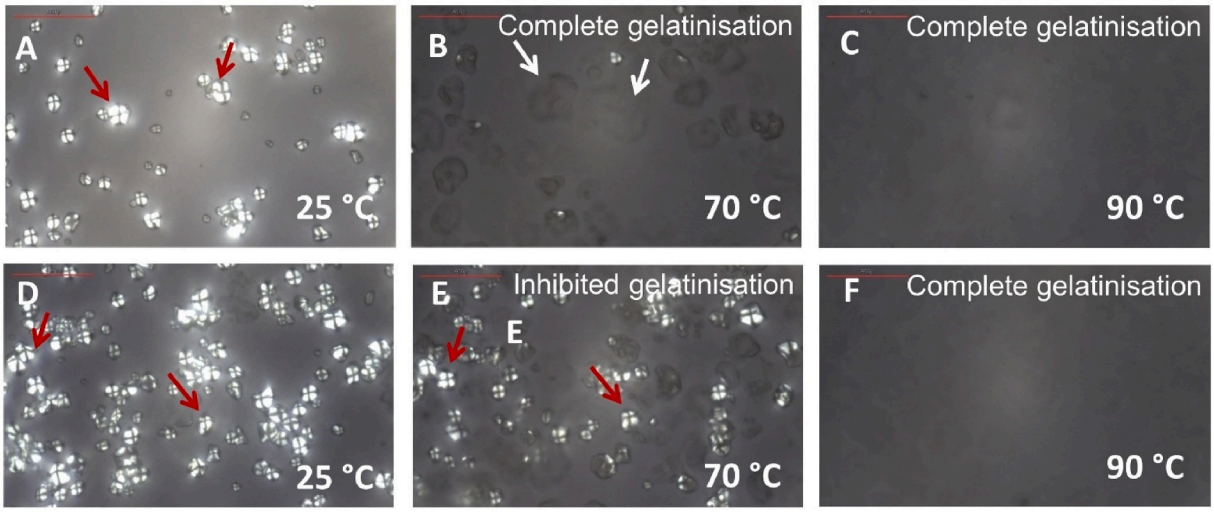

Fig. 2. Polarised micrographs of waxy corn starch at 0.50 %, w/w at 25 °C (A, D), waxy corn starch + soluble amylose chain (DP 704, 25W) at 1 %, w/w at 70 °C (B, E), and waxy corn starch + soluble amylose chain (DP 704, 25W) at 1 %, w/w at 90 °C (C, F). In 25W, 25 refers to the temperature in °C at which the fraction was collected, whereas W refers to the origin of the fractions, waxy corn starch variety. In figures, red arrows are visual guide to indicate examples of granules with birefringence at 25 °C which continued to resist loss of birefringence at 70 °C, while white arrows are a visual guide to indicate examples of granules which lost birefringence at 70 °C. Video showing granular loss of birefringence as a function of temperature rise from 25 → 95 °C is in Supplementary Video SV1. (For interpretation of the references to colour in this figure legend, the reader is referred to the Web version of this article.)

findings from calorimetry. It is clear that soluble amylose chains lead to inhibition of waxy corn starch gelatinisation, however this inhibition is not complete and does not result in a full cessation of the gelatinisation process.

3.3. Effects of soluble amylose chains on the pasting properties of waxy corn starch

As gelatinisation and retrogradation are known to be strongly correlated (Balet et al., 2019; Fu et al., 2013), we additionally probed the effect of adding soluble amylose chains on the swelling, pasting, and short-term retrogradation properties of waxy corn starch. Complete pasting curves for all pure waxy corn starch, waxy corn starch-maltose/maltodextrin, and waxy corn starch-soluble amylose chains are shown in Supplementary information, Fig. S3A–G and Table S3. We lay special emphasis on the pasting temperature, and peak, trough, and final viscosities in our analyses, and are shown in Fig. 3A–D. Note, pasting temperature correlates with temperature required for gelatinisation, peak viscosity correlates to the water uptake or holding capacity of the systems, the trough viscosities correlates to the extent of granular disassembly under the applied shear stress, and final viscosities are indicative of the extent of retrogradation during the cooling phase. Pasting time, peak time, breakdown viscosities, and total setback are shown in Supplementary Information, Fig. S4A–D.

The pasting temperature of pure waxy corn starch remains independent of starch concentration (within the range of 5–10 wt%), remaining at ca. 75 °C indicating that the onset of the pasting is not affected by the variation in the solid content and the water excess is sufficient to render any water deficit effect negligible. By contrast, pasting temperature for waxy corn starch-soluble amylose chain mixtures increased from 75 to 79 °C for DP 186, to 79 °C for DP 216, to 81 °C for DP 704, and to 79 °C for DP 4020. Across all DPs, where the onset of gelatinisation was observed in our calorimetry experiments, we observe a ca. 5 °C increase in the gelatinisation temperature at the solid content level, where effects of water deficit remain small. For two comparator samples, maltose (DP 2) and maltodextrin (DP_{avg} 20), no changes were observed in pasting temperatures for waxy corn starch-maltose/maltodextrin mixtures. These observations illustrate that at low concentrations of soluble materials, where effect of osmotic pressure is minimal, the addition of soluble amylose chains to waxy corn starch has a distinctive mechanism through which the thermal requirement for granular swelling in the mixture increases. Taken together, the RVA and DSC results point towards a unique way the soluble amylose chains effect starch gelatinisation. We note that solutions of fraction on their own have viscosity very similar to that of water, which is reflective of their low molecular weight.

Our results echo the observations reported by Gong and coworkers (Gong et al., 2024), where delay in wheat starch pasting was observed upon addition of pullulan (M_w, 3–300 kDa). However, our results are contrary to the findings of Krystyjan and coworkers (Krystyjan et al.,

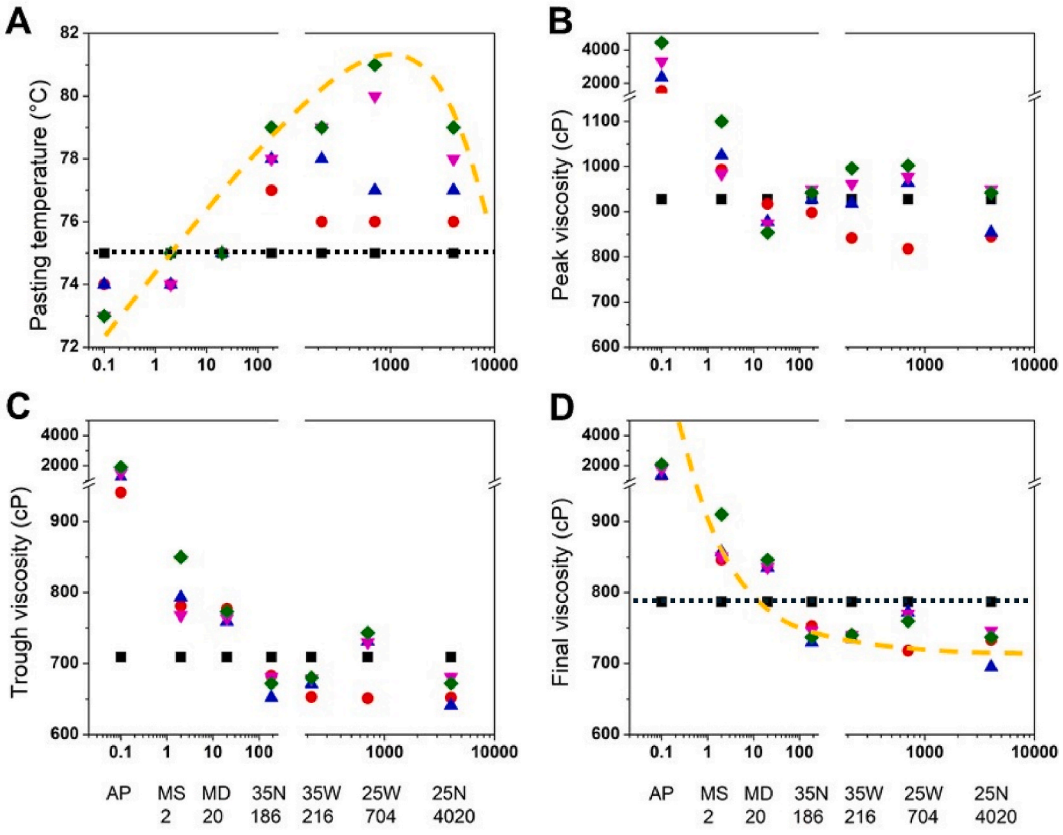

Fig. 3. Pasting temperature, peak viscosity, trough viscosity, and final viscosity as a function of degree of polymerisation, DP (A–D) of waxy corn starch + water and waxy corn starch + additive + water systems. Mixing ratios are indicated as, 1:0 (■), 1:0.25 (●), 1:0.50 (▲), 1:0.75 (▼) and 1:1 (♦) corresponding to 95 %, 93.75 %, 92.5 %, 91.25 % and 90 % water content, respectively. Black dashed line is a visual guide to indicate pure waxy corn starch behaviour. Orange dashed line is a visual guide indicating (A) initial increase in pasting temperature as chain DP increases, which eventually decays, and (D) pseudo-exponential decay and plateauing of final viscosity with the increase in chain DP. AP denotes waxy corn starch and is plotted for comparison and does not indicate a DP of ~0.1. MS, maltose (DP 2); MD, maltodextrin (DP 20); 35N (DP 186); 35W (DP 216); 25W (DP 704); 25N (DP 4020). In soluble amylose chains (35N, 35W, 25W, and 25N), 25 and 35 refer to the temperature in °C at which the fractions are collected, whereas N and W refer to the origin of these fractions, either native or waxy corn starch varieties. Raw data is shown in Supplementary Information, Fig. S3A–G and exact estimates are shown in Table S3. Related pasting time, peak time, trough viscosities, and total setback are shown in Supplementary information, Fig. S4A–D. (For interpretation of the references to colour in this figure legend, the reader is referred to the Web version of this article.)

2022), where significant early onset in the initial pasting temperature was observed when xanthan was added to native and waxy corn starch.

In addition to effects on the pasting temperature, we explored the effect of soluble amylose chains on peak viscosity, which is associated with the polymeric nature of these material that give rise to the additional, purely hydrodynamic effects associated with higher viscosity of the continuous phase in the presence of soluble amylose chains. The peak viscosity increased from 928 to 942 cP for DP 186, to 996 cP for DP 216, to 1002 cP for DP 704, and to 942 cP for DP 4020 soluble amylose chain addition. An increased from 928 to 1100 cP was observed for waxy corn starch-maltose, while for waxy corn starch-maltodextrin system the peak viscosity decreased from 928 to 854 cP. The changes in peak viscosity with addition of soluble starch-derived components is minimal in comparison with an increase in peak viscosity for pure waxy corn starch, where the peak viscosity increased from 928 to 4446 cP when the waxy corn starch content increased from 5 to 10 wt%.

The increase in the peak viscosity in the presence of soluble amylose chain DP correlates with the increase of DP for DP $\leq$ 1000, which would be consistent with increase in the soluble amylose chain phase volume associated with the increase in molecular weight. However, for DP $\geq$ 1000, the effect of viscosity diminished, indicating that the amylose chain may become less hydrated as their solubility decreases. In another words, with the increase in DP the soluble amylose chains attain characteristics of native high molecular weight amylose chains that have poor water solubility.

The solubility argument can potentially explain the apparent discrepancy between our results and those of Krystyjan and coworkers (Krystyjan et al., 2022), where xanthan, a high molecular weight extracellular bacterial polysaccharide, was utilised. In addition, it is worth mentioning other reports where starch gelatinisation was probed in the presence of other high molecular weight hydrocolloids, such as pullulan (Chen et al., 2014) and sugar beet pectin (Xu et al., 2023). For all highly soluble hydrocolloids, the peak viscosity decreased due to the reduction of the swelling volume during pasting. This is consistent with our results for highly soluble amylose chains with DP $\leq$ 1000, where an increase in DP led to a decrease in peak viscosities in the mixtures (Fig. 3B). Our results for trough viscosities are also in agreement, showing an increase from 709 to 1886 cP for waxy corn starch, 709 to 850 cP for waxy corn starch-maltose gels, and 709 to 773 cP for waxy corn starch-maltodextrin. However, trough viscosities decreased as soluble amylose chain DP increased. These results demonstrate that both granular swelling and mechanical breakdown were restricted by the presence of soluble amylose chains.

Once gelatinised, cooling induces a disorder → order phase transition in starches and is known as starch retrogradation. We therefore examined the final viscosities for our systems, and are shown in Fig. 2D and Supplementary Information, Table S3. In our samples, the final viscosity increased from 787 to 2082 cP for waxy corn starch, 910 cP for waxy corn starch-maltose, and 910 cP waxy corn starch-maltodextrin, however decreased from 787 to 737 cP for DP 186, to 740 cP for DP 216, to 760 cP for DP 704, and to 737 cP for DP 4020. It appears that soluble amylose chains have an inverse correlation amidst DP and retrogradation, as was also observed for gelatinisation. Note, corresponding total setback, *i.e.*, the difference of the final viscosity from the trough viscosity, are shown in Supplementary information, Fig. S4D and Table S3.

Since our final viscosities were restricted by a lower temperature limit of 50 °C in our calorimetry experiments, we provide further evidence about the ability of soluble amylose chains to induce inhibition of retrogradation in waxy corn starch using turbidity analysis. Note, temperatures were reduced back to 20 °C in the turbidity analyses measurements without application of any shear stress. In these analyses, retrogradation was expected to induce water syneresis and promote crystallization of starch chains, leading to a more ordered and compact network. This structural reorganisation was expected to enhance settling of the starch phase, thereby resulting in an increased transmission of light. Fig. 4 shows transmission as a function of DP. We observed that at

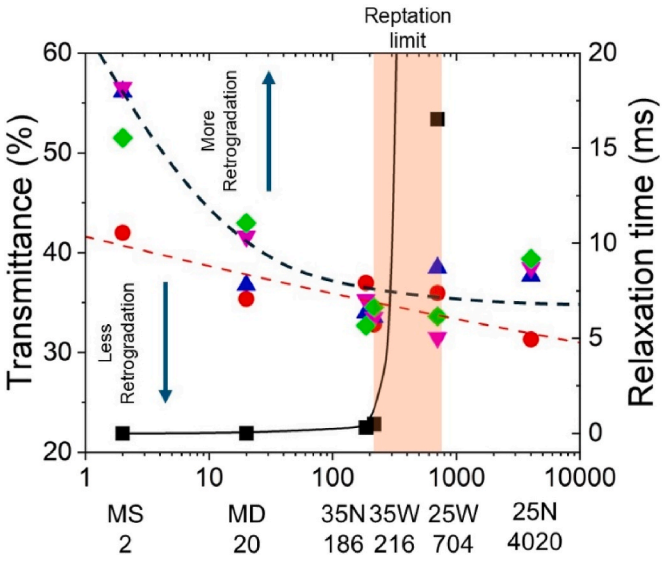

Fig. 4. Transmission and relaxation time as a function of degree of polymerisation of soluble amylose chains and the comparators. Transmission % is from turbidity analysis. Relaxation time refers to the terminal (reptation) relaxation time. Here, increasing addition of soluble amylose chains to waxy corn starch granules is indicated as waxy corn starch: soluble amylose chain: 1:0.25 (●), 1:0.50 (♦); 1:0.75 (▼); 1:1 (▲). MS, maltose (DP 2); MD, maltodextrin (DP ~ 20); 35N (DP 186); 35W (DP 216); 25W (DP 704); 25N (DP 4020). In soluble amylose chains (35N, 35W, 25W, and 25N), 25 and 35 refer to the temperature in °C at which the fractions are collected, whereas N and W refer to the origin of these fractions, either native or waxy corn starch varieties. Note, log transmittance (%) is a representation of log of transmittance (%), where transmission (%) values 0–100, equals 0–2 log transmission (%) values. Raw data is shown in Supplementary Information, Fig. S5. Red dashed line indicates a power law fit. Black dashed line is a visual guide indicating pseudo exponential decay. Solid black line is a spine function, and the data for DP4020 is outside the bounds of the relaxation time axis for illustrative purposes. Reptation limit denotes the soluble amylose chain entanglement limit (200 $\leq$ DP $\leq$ 700). (For interpretation of the references to colour in this figure legend, the reader is referred to the Web version of this article.)

lower addition ratios, *i.e.*, 1:0.25 (waxy corn starch: soluble amylose chain), an increase in soluble amylose chain DP leads to a decrease in starch retrogradation and can be described by a 'weak' power law relationship as, $retrogradation \propto DP^{0.04}$ (Fig. 4, red dashed line represents the power law model). However, when the incorporation of soluble amylose chains in waxy corn starch was sequentially increased to 1:1 ratio, this relationship appears to break down. We cautiously state the observed retrogradation behaviour as pseudo-exponential decay (Fig. 4, black dashed line is a visual guide). An initial decrease in retrogradation was evident till DP $\leq$ 216. However, this tends to plateau upon incorporation of soluble amylose chains with higher DP $\geq$ 700 *i.e.*, 25W and 25N. Further increase in DP $\geq$ 700 does not appear to decrease retrogradation. Our results closely corroborate the findings of final viscosity and consolidates the inverse relationship between DP and retrogradation. Soluble amylose chain DP in the range of 200–700 *i.e.*, samples 35W–25W appears to be the 'critical chain length' which leads to highest retardation of retrogradation in waxy corn starch and is closely concentration dependant. This behaviour is also somewhat consistent with gelatinisation (please see orange dashed line in Fig. 3A–D). Our results demonstrate that 'short' soluble amylose chains (*i.e.*, DP $\leq$ 1000) are sufficient to inhibit both gelatinisation and short-term retrogradation in waxy corn starch.

But why does a critical chain length exist? Collectively, the observations from calorimetry and turbidity analysis, indicates towards a DP-dependent inhibition mechanism. Therefore, we now provide a mechanistic interpretation using the Rouse → reptation crossover to ratio-

nalise and identify a reptation limit, by virtue of which increasing DP leads to the plateauing behaviour in both gelatinisation and retrogradation for DP ≥ 200. The reptation (entangled) diffusion for a typical entanglement length $N_e \approx 120$ for flexible amylose chain may be expressed as $D_{reptation} = D_R N_e/N$, where N = chain DP and N_e for linear α-1,4-*d*-glucans is derived from the molecular-weight between entanglements, M_e, where $N_e = M_e/162\left(\text{g mol}^{-1}\text{per glucose}\right) \approx 120–180$, where $M_e = 2–3 \times 10^4$ (Horinaka et al., 2011, 2012; Li et al., 2022). Note, 162 g mol^{-1} per glucose corresponds to anhydrous glucose in an amylose chain, where the formation of glycosidic linkages involves the elimination of water molecules from the original glucose monomer. For the soluble amylose chain the reptation diffusion therefore follows the order: 35N (DP 186) > 35W (DP 216) ≫ 25W (DP 704) ≫ 25N (DP 4020) (Table 3). Thus, the effective diffusion coefficients scale inversely with DP with N^{-2}. Osmanović (Osmanović, 2018) describes the expression for the internal Rouse relaxation time for the whole chain (longest mode, $p = 1$) as $\tau_R = \frac{\zeta b^2 N}{3\pi^2 k_b T}$. Considering Rouse (reptation) time, this relationship translates to, $\tau_e = \tau_R(N_e)$, therefore, the terminal (reptation) relaxation time for the soluble amylose chains may be expressed as, $\tau_d = \frac{\zeta b^2}{3\pi^2 k_b T}\frac{N^3}{N_e}$, where $\tau_d = \tau_e\left(N/N_e\right)^3$. Note, the Stokes radius of a single glucose unit in the amylose chain was considered as the Kuhn length parameter, *b* as a one-parameter coarse-graining approach, and is supported by other reports where amylose derivates evidence a Kuhn length of ca. 0.45 nm (Kühner et al., 2006). From Table 3 it is evident that the terminal relaxation time for soluble amylose increases from 3.05×10^{-4} s for DP 186 (35 N) to 0.02 and 3.08 s, *i.e.* a 2- and 4-orders of magnitude increase for DP 704 (25W) and DP 4020 (25 N), respectively. This marked slowdown in terminal relaxation time of the soluble amylose chains is shown in Fig. 4 and corroborates with the plateauing of transmission % as chain DP reaches a reptation limit *i.e.*, 200 ≤ DP ≤ 700 (Fig. 4). Therefore, a 'critical chain length' must exist around 200 ≤ DP ≤ 700, beyond which chains can no longer penetrate the interior of the granules due to the dominant chain entanglement.

Table 3
Reptation diffusion and relaxation time of the soluble amylose chains.

Soluble amylose chains	DP	Chain friction $\zeta = N\zeta_0$	Reptation: Diffusion $D_{reptation} = D_R \cdot N_e/N$	Reptation: Terminal relaxation time, τ_d
		kg s^{-1} × 10^{-6}	m^2 s^{-1}	ms
Maltose	2	0.01	NA	NA
Maltodextrin	20	0.12	NA	NA
35N	186	1.19	2.75×10^{-15}	3.05×10^{-1}
35W	216	1.38	2.04×10^{-15}	4.77×10^{-1}
25W	704	4.49	1.92×10^{-16}	1.65×10^{1}
25N	4020	25.66	5.88×10^{-18}	3.08×10^{3}

Degree of polymerisation (DP). 25W and 35W: soluble amylose chains extracted at 25 °C and 35 °C, 'W' indicates waxy corn starch source; 25N and 35N: soluble amylose chains extracted at 25 °C and 35 °C. N indicates native corn starch source. For calculations of chain friction parameter (ζ), Rouse (reptation) diffusion coefficient ($D_{reptation}$), and terminal (reptation) relaxation time at the temperature of the fully gelatinised state (T = 93 °C), the following parameters and relationships were used: Boltzmann constant, $k_B = 1.38 \times 10^{-23}$ J K^{-1}, monomer friction, $\zeta_0 = 6\pi\eta_s d \approx 6.38 \times 10^{-9}$ kg s^{-1}, Stokes radius of glucose unit, $d \cong 3.6$ Å (Bouchoux et al., 2005), solvent viscosity, η_s ~928 cP (taken as peak viscosity of waxy corn starch gels), N = DP, and Rouse diffusion was estimated as $D_R = K_B T/\zeta$. Chain friction (ζ) refers to the total chain friction. Rouse diffusion for maltose and maltodextrin are estimates as 3.96×10^{-13} and 3.96×10^{-14} m^2 s^{-1}, respectively. Reptation diffusion could not be estimated for maltose and maltodextrin as, DP ≤ N_e. Short oligomers therefore appear to diffuse 2 - 3 orders of magnitude faster compared to the soluble amylose chains. Samples are arranged in ascending order of their DP. NA, not applicable.

3.4. Interaction between soluble amylose chains and waxy corn starch granules

Based on our results on the existence of a 'critical chain length', we probe the waxy corn starch-soluble amylose chain mixture to investigate any chain adsorption on waxy corn starch granule surfaces, using fluorescence microscopy. We used 25W (DP 714) as the model soluble amylose chains for the analysis, as 25W represents the critical DP at which retrogradation of waxy corn starch plateaus and was therefore expected to provide clear account of adsorption.

Soluble amylose chains were labelled with the fluorescent dye, 5-DTAF (λ_{ex}, 470 nm, λ_{em}, 525 nm). Any adsorption of labelled-soluble amylose chains onto the waxy corn starch granules would tangibly increment the fluorescence density of the granules. Note, samples were imaged after thermal treatment at 95 °C. Cues for this temperature came from our earlier polarised light microscopy experiment and ensured that soluble amylose chain-waxy corn starch mixtures undergo complete gelatinisation. This allowed us to monitor both adhesion and granular swelling/disassembly. As seen from the micrograph, 5-DTAF-waxy corn starch are marked with structural heterogeneity typical for a gelatinised starch matrix (Fig. 5A). Fig. 5B shows the 5-DTAF-soluble amylose chains as a completely homogenous system, quite expected for water-soluble polymer chains. In contrast, granular morphology was still apparent in 5-DTAF-soluble amylose chain - unlabelled waxy corn starch mixtures (Fig. 5C and D), and is concurrent with our results from polarised light microscopy on inhibited gelatinisation. In the 5-DTAF-soluble amylose chain – unlabelled waxy corn starch mixtures, the fluorescence intensity of starch granules appears to be amplified after incorporation of soluble amylose chains. This increase in fluorescent density is ca. 45 % higher compared to the background and was measured on Fig. 5D using ImageJ (NIH, USA). Other results from fluorescence time-series imaging also evidences a largely uniform fluorescence signature at $t = 0$ min, implying that 5-DTAF-soluble amylose chains remains predominantly in the continuous phase and has not yet adsorbed appreciably to the waxy corn starch granules (Fig. 5E). Contrarily, at $t = 5$ min, one could clearly observe adsorption of the 5-DTAF-soluble amylose chains on to the granule surfaces, signifying rapid adsorption of soluble amylose chains onto waxy corn starch granule surfaces (Fig. 5F). A video of this rapid adsorption process is shown in Supplementary Information, Video SV2.

Based on the results and earlier arguments on reptation diffusion and terminal relaxation time, it is clear that the 5-DTAF-soluble amylose chains adsorbs on the starch granule surface, without percolation into the granules. The current findings are concurrent with our previous reports, where amylose fractions were observed to form nanometre thick films (~2 nm) on the surface of insoluble starch particles (Yakubov et al., 2015). We illustrate this plausible mechanism in Fig. 6, where soluble amylose chains adsorb onto the granule surfaces, envelops the granules, and results in inhibited gelatinisation and granular disassembly.

To probe the structural effects of spontaneous adsorption of soluble amylose chains and to deepen our understanding of their inhibitory effect on waxy corn starch gelatinisation, we utilised small-angle X-ray scattering (SAXS) and wide-angle X-ray diffraction (XRD). For pure waxy corn starch at 20 °C, we observed a characteristic SAXS peak positioned at q_{max} ~0.60 nm^{-1}, which is widely accepted to originate from the stacking order in the semi-crystalline regions of starch granules, alongside an A-type monoclinic crystalline structure with prominent XRD peaks at 2θ (λ = 0.154 nm) 15°, 17°, 17.8°, and 22.8°, corresponding to the *q* values of 10.65, 12.14, 12.77, and 16.26 nm^{-1}, respectively (Fig. 7A–C; Tables 4 and 5). Both observations are consistent with previous reports (Borah et al., 2017, 2019b; Chen et al., 2017). Pure soluble amylose chains displayed the expected characteristic

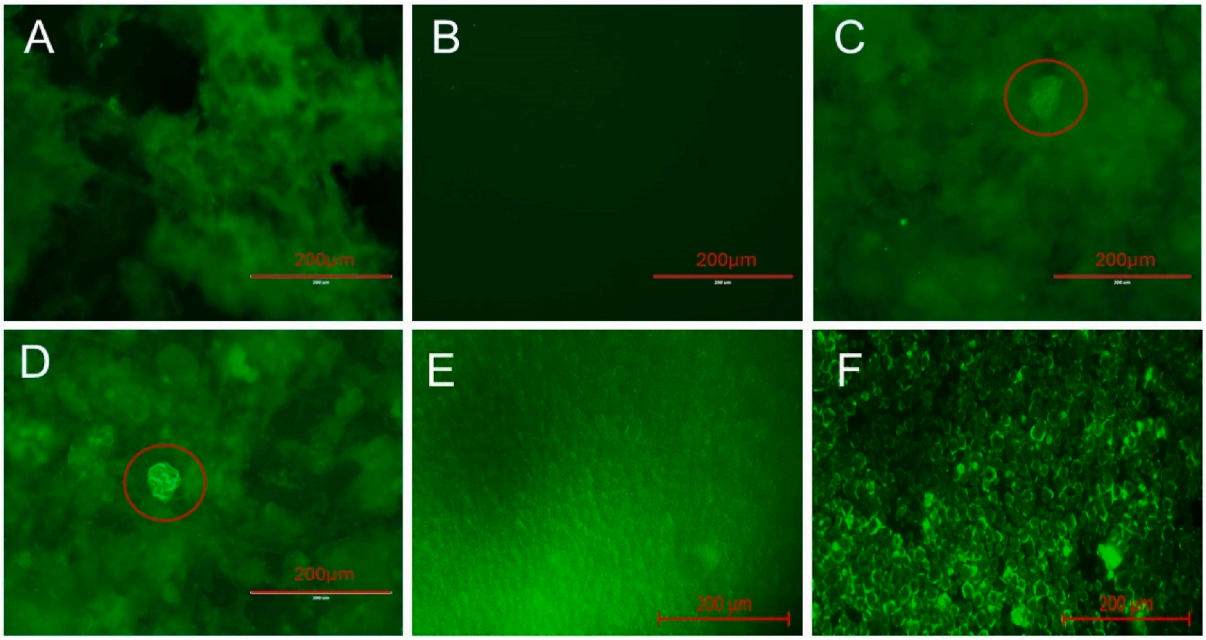

Fig. 5. Fluorescent micrographs of 5-DTAF-waxy corn starch gel at 4 %, w/w (A); 5-DTAF-soluble amylose chain (DP 704) at 1 %, w/w (B); unlabelled waxy corn starch + 5-DTAF-soluble amylose at 5 %, w/w at 400X magnification (C–D). Red circles are a visual guide to indicate swollen but intact granules of unlabelled waxy corn starch, where the fluorescence intensity is amplified by the adsorption of 5-DTAF-soluble amylose chains. Fluorescent micrographs recorded during the time series experiment: unlabelled waxy corn starch + 5-DTAF-soluble amylose chains at time, t ~0 min (E) and at time, t = 5 min (F). λex, 470 nm, λem, 525 nm. Scale bars are 200 µm. Video showing DTAF-soluble amylose chain adsorbing onto waxy corn starch granule surfaces is shown in Supplementary Information, Video SV2. (For interpretation of the references to colour in this figure legend, the reader is referred to the Web version of this article.)

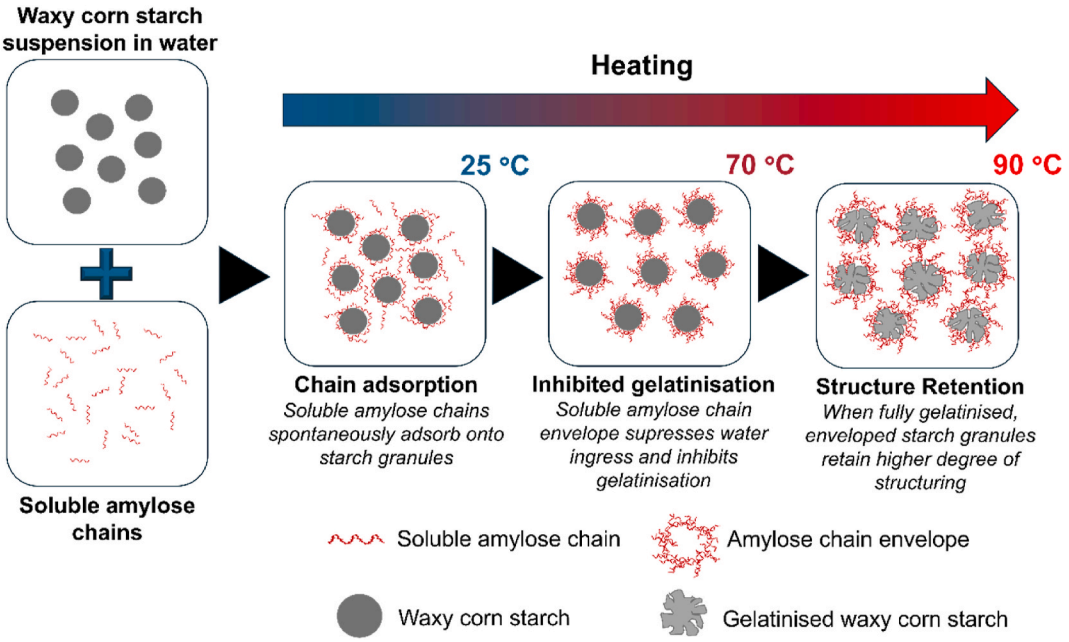

Fig. 6. Schematic illustration of soluble amylose chains adsorption on to waxy corn starch granule surfaces and the effect on the gelatinisation. (The temperature values correspond to the data presented in Fig. 2 and in Supplementary Video SV1.) We postulate that soluble amylose adsorbs onto the granule surface leading to the formation of an enveloped starch granule. The amylose chain envelope features 'V-type' polymorphism structuring. It restricts water ingress and/or dehydrates starch granules leading to inhibited gelatinisation and restricted granular disassembly, even at elevated temperatures.

V-type polymorphism (Fig. 7C; Table 5). Upon mixing soluble amylose chains with waxy corn starch, the SAXS scattering pattern did not reveal any emerging structural features in the q-range <1.5 nm^{-1} (Fig. 7B). However, the diffraction pattern was markedly distinct. Although it appears to bear features of both A-type and V-type polymorphisms, the diffraction pattern is not a trivial superposition of the two. While the features corresponding to waxy corn starch are largely preserved, the V-type features underwent a marked change. The most prominent peak emerged at *2θ, 11.46°*, with smaller peaks at *2θ, 17°* and *22.5°* (Fig. 7C), which we attribute to V-type-like structures of amylose in the surface layer surrounding the starch granules.

To monitor the gelatinisation process, we heated samples from

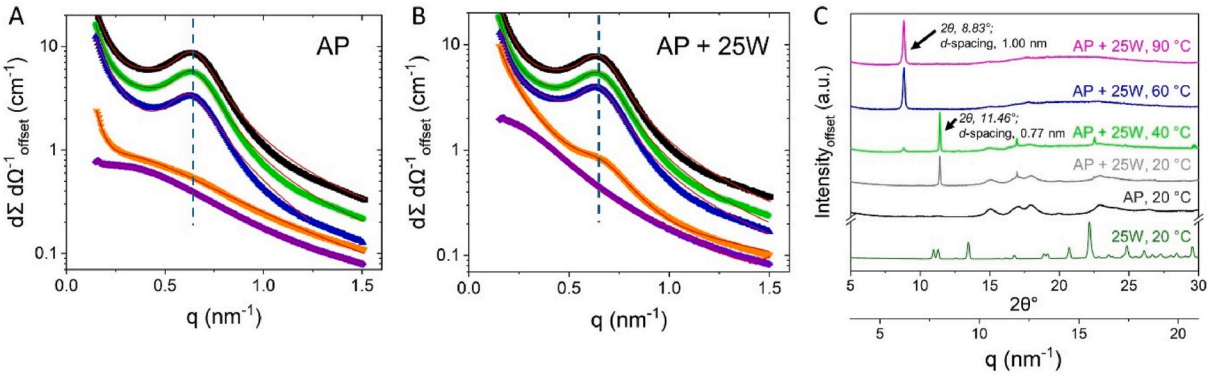

Fig. 7. Background subtracted small-angle X-ray scattering (SAXS) spectra as a function of q ($\lambda = 0.1314$ nm) and fitted model functions (—) for (A) waxy corn starch, AP, and (B) waxy corn starch + soluble amylose chain, AP + 25W (1:0.5 ratio) recorded at varying temperatures: 20 °C (■), 40 °C (●), 60 °C (▲); 80 °C (▼); 90 °C (♦). Black dashed lines are a visual guide to indicate the starch lamellar repeat distance, $d = 9$–10 nm. (C) Wide-angle X-ray diffraction (XRD) spectra of the samples as a function of 2θ ($\lambda = 0.154$ nm) and q ($\lambda = 0.1314$ nm): soluble amylose chain with DP 704 (25W) at 20 °C (dark green); waxy corn starch (AP) at 20 °C (black); waxy corn starch + soluble amylose chains with DP 704 (AP + 25W) at 20 °C (dark grey); waxy corn starch + soluble amylose chains with DP 704 (AP + 25W) at 40 °C (green); waxy corn starch + soluble amylose chains with DP 704 (AP + 25W) at 60 °C (blue), and waxy corn starch + soluble amylose chains with DP 704 (AP + 25W) at 90 °C (magenta). All samples were hydrated to a paste-like consistency with 100 μL of water before the experiment. d-spacing were calculated using the relationship $q \sim 2\pi/q$. Black arrows indicate the shift in 'V-type'-like polymorphism with temperature change. (For interpretation of the references to colour in this figure legend, the reader is referred to the Web version of this article.)

Table 4
Structural parameters of the semi-crystalline region deduced from the SAXS data.

		Structural parameters				
Temperature	Samples	q_{max}	d	Δq	HWHM	δ
°C		nm^{-1}	nm	nm^{-1}	nm	
20	AP	0.64	9.82	0.13	2.04	2.22
40		0.64	9.85	0.13	2.14	2.50
60		0.62	10.07	0.14	2.39	1.93
80		ND	ND	ND	ND	1.68
90		ND	ND	ND	ND	1.03
20	AP-25W	0.64	9.75	0.125	2.01	2.26
40		0.64	9.81	0.13	2.12	2.51
60		0.64	9.82	0.13	2.04	2.35
80		0.65	9.61	0.155	2.45	1.88
90		ND	ND	ND	ND	1.38

AP, waxy corn starch; AP-25W, waxy corn starch-soluble amylose. ND, not detected; δ, Porod exponent.

Table 5
Crystallinity characteristics of waxy corn starch upon addition of soluble amylose chains.

Temperature	Samples	Relative crystallinity	Peaks	Polymorph
°C		%	2θ°	
20	AP	34	15, 17, 17.8, 19.8, 22.8	A-type
20	25W	97	11, 13, 19, 20, 22, 24, 26, 27, 28, 29	V-type
20	AP-25W	40	11.46, 15, 17, 18, 20, 22.50, 23	A-type, V-type*
40		22	8.82, 11.34, 15, 17, 22.5	A-type, V-type*
60		24	8.83	V-type*
90		22	8.83	V-type*

AP, waxy corn starch; AP-25W, waxy corn starch-soluble amylose. Corresponding XRD spectra are shown in Fig. 7C. *The V-type polymorph is unlike the conventional V-type polymorph typically observed in starch XRD studies.

20 → 90 °C. At 40 and 60 °C, the characteristic SAXS peak at d ~9 nm, corresponding to the lamellar structures of waxy corn starch, retained its prominence. As evidenced by the increase in HWHM (Table 4), some broadening of the peak reflects the progression of lamellar swelling and hydration of amorphous regions (Waigh et al., 2000); however, the magnitude of this effect appears to be small. Upon further heating to 80 °C, the characteristic lamellar peak for waxy corn starch fell below the detection limit (Fig. 7A), suggesting that roughly 75 % of the semi-crystalline volume had melted (ca. $\leq 0.25\ I_0$). Under the same conditions, the semi-crystalline region of the waxy corn starch-soluble amylose chain mixture was not eliminated, and a measurable reflection at q, 0.65 nm^{-1}, corresponding to a d-spacing of 9.61 nm, persisted (cf. Fig. 7A and B). Notably, the remaining intact semi-crystalline regions displayed almost identical stacking density (d-spacings,Table 4), while showing an appreciable increase in local stacking disorder (Δq and HWHM values,Table 4). This indicates that granule swelling and hydration of amorphous regions in the mixed system were markedly different compared to pure waxy corn starch. At 90 °C, both waxy corn starch and the waxy corn starch-soluble amylose chain mixture showed complete melting of starch lamellar stacks.

In parallel with lamellar melting analysis, Porod law deviations from $I(q) \sim q^{-\delta}$ were used for fractal analysis. The low-q region in our scattering profiles was representative of the lamellar structure of starch growth rings, in agreement with scattering studies of waxy corn starch by Mao and coworkers in the range, $0.1 \leq q \leq 0.3\ nm^{-1}$ (Mao et al., 2023). For both waxy corn starch and the waxy corn starch-soluble amylose chain mixture, the exponentially decaying diffuse scattering contribution strongly decreased, though not identically (note, identical exposure times were applied). The values of δ started at ca. 2.20 for both samples at 20 °C and progressively diverged to 1.03 and 1.38 at 90 °C, respectively. This progression suggests that both samples initially exhibited scattering characteristics indicative of a high-dimensional mass fractal structure ($2 \leq \delta \leq 3$). Following gelatinisation, the structure transitioned to a low-density mass fractal gel structure, as evidenced by the markedly lower Porod exponent ($\delta \sim 1$). Importantly, the waxy corn starch-soluble amylose chain mixture showed a slower decay of δ compared to waxy corn starch (δ values, Table 4). Taken together with the lamellar spacing data, the Porod behaviour highlights the distinct inhibition of temperature induced structural transitions in the waxy corn starch-soluble amylose chain mixtures.

By probing the gelatinisation behaviour using XRD, we observed a

decay in A-type polymorphism accompanied by an increase in 'V-type' polymorphism. At 40 °C, the increased intensity of the 2θ, 11.46° peak (q, 8.14 nm^{-1}) was accompanied by the emergence of a new diffraction peak at 2θ, 8.83° (q, 6.27 nm^{-1}) (Fig. 7C). As the temperature was further increased to 60 °C, the reflection at 2θ, 8.83° became more prominent, while the 2θ, 11.46° reflection disappeared entirely. The former peak is a stronger reflection that corresponds to Miller indices $h = 0$ and $k = 1$. Conversely, during this process, the first-order d-spacing increased from 0.77 to 1.00 nm, which constitutes a ca. 30 % increase. Popov and coworkers (Popov et al., 2009) reported the presence of two water molecules per maltotriosyl unit in the crystal structure of A-amylose (CCDC Deposition Number: 1019243), whereas Sarko and Biloski (Sarko & Biloski, 1980) described an amylose structure complexed with three water molecules per triosyl unit, presenting an extended conformation (CCDC Deposition Number: 193097). We simulated the powder diffraction patterns of both CCDC entries (Supplementary Information, Fig. S6). The structure with two water molecules shows a characteristic reflection at 2θ, 11.37° (q, 8.08 nm^{-1}), while the structure with three water molecules shows a characteristic peak at 2θ, 8.19° (q, 5.82 nm^{-1}). Although a shift in a single diffraction peak is insufficient to draw firm conclusions, it suggests that at elevated temperatures, these polymorphic transitions likely arise from the intercalation of water molecules into the interior of soluble amylose chain helices. We also examined the sample at 90 °C, which continued to exhibit a strong 2θ, 8.83° reflection (Table 5).

In summary, we propose that at the critical chain length ($200 \leq DP \leq 700$), soluble amylose chains exhibit reduced terminal relaxation time which prevents their ingress into the interior of starch granules - unlike smaller sugars and oligomers. This leads to the formation of a 'V-type' amylose coat that envelops the starch granule surfaces. We postulate that this amylose envelop absorbs available water, effectively dehydrating the granules or restricting water ingress. The reduction in available water inside the granules interferes with starch-water interactions, suppressing lamellar melting and consequently inhibiting gelatinisation. Consistent with the requirement for water molecules to melt starch lamellar structures, Yang and coworkers demonstrated that starch granules in non-polar solvents such as ethanol do not lose their lamellar and fractal structure in SAXS studies (Yang et al., 2016), underscoring the crucial role of water in lamellar melting.

Conversely, the persistence of amylose structures at higher temperatures - when starch is fully gelatinised - and the presence of partially structured regions contribute to the reduction of the molecular mobility, which consequently has an inhibitory effect on short-term retrogradation. Our observations align with the findings of Fu and coworkers (Fu et al., 2013), who reported that retrogradation correlates with the initial degree of gelatinisation in corn starch. Further studies are underway to investigate these considerations and will be presented in a future report.

4. Conclusions and future perspectives

Soluble amylose chains inhibit both gelatinisation and short-term retrogradation in waxy corn starch granules. Soluble amylose chains with a degree of polymerisation (DP) in the range of 200–700 appear to present the 'critical chain length' that shows the highest inhibition of gelatinisation and retrogradation in waxy corn starch, and this effect is concentration dependent. While previous theories regarding the effect of mono-, di- and oligosaccharide on the inhibition of starch gelatinisation associated with their penetration into starch granules may hold true for lower DP additives (*i.e.*, $DP \leq 200$), we argue based on the reptation (entangled) limit - that such penetration is unlikely for soluble amylose chains, especially as their DP approaches the 'critical chain length' of $200 \leq DP \leq 700$.

We propose that the formation of the coating occurs via physical adsorption of soluble amylose chains onto the starch surface. However, based on the marked dissimilarity between the XRD patterns of pure amylose chains and those observed when the chains are deposited on starch granules, we corroborate that during adsorption, the chains undergo structural transformation and form a new type of 'V-type'-like amylose structuring. Such a structured surface coating may inhibit gelatinisation through several mechanisms: a) reduction of available water required for starch gelatinisation and restriction of water migration into the granule interior; b) formation of a gel-like layer that physically restricts granular swelling and disassembly, thereby affecting starch pasting properties (Alshammari et al., 2024); c) reduction in chain mobility, which affects molecular rearrangement, including during short-term retrogradation. Importantly, all these mechanisms result in a higher proportion of ordered structures that persist in gelatinised starch coated with soluble amylose chains. These structural changes, alongside techno-functional properties, may also influence the nutritional characteristics of starch.

However, despite the in-depth analyses presented in this investigation, several open questions remain: What are the adsorption isotherms for soluble amylose chain deposition on waxy corn starch granule surfaces? What is the thickness of the soluble amylose layer on granule surfaces, and how does it relate to delayed gelatinisation and retrogradation? What is the effect of soluble amylose chains on the gelatinisation and retrogradation of starch granules from other botanical sources? The results presented in this article - particularly regarding short-term retrogradation - also provide valuable insights for future studies on long-term retrogradation in soluble amylose chain-waxy corn starch systems, as well as for investigations into the digestion behaviour of these mixed systems. Further studies are needed to address these questions and deserve attention in future research.

Our findings also open several promising avenues for food processing, as well as applications in controlled-release pharmaceuticals, edible coatings, and advanced biomaterial 3D printing. In food systems, blending corn starches with short soluble amylose chains can offer functional advantages in terms of industrial process optimisation and enhanced resilience. For example, in soups, sauces, and gravies, delayed gelatinisation allows for longer holding times at mid-range temperatures (~50 °C) without premature thickening or clumping (Chakraborty et al., 2022). Inhibition of short-term retrogradation reduces or prevents syneresis, ensuring more consistent viscosities and maintaining pumpability after heating-cooling cycles (Zhang et al., 2019). An increase in pasting temperature enables greater flexibility in high-temperature processing without compromising granular structure and avoiding its excessive breakdown (Hsieh et al., 2019). From a sensory and oral processing perspective (Boehm et al., 2019, 2020), short soluble amylose chains may reduce staling and contribute to smoother, creamier textures - beneficial for baked goods, crackers, sauces, custards, puddings, and dairy analogues based on plant-based or alternative protein ingredients (Kew et al., 2021). Furthermore, in formulations such as batters or extruded snacks, inhibited retrogradation can help delay gelling, maintain fluidity during processing or extrusion, and prevent premature viscosity spikes (Ren et al., 2021). Ideally, manufacturers could fine-tune viscosity profiles across various short soluble amylose-starch blends to delay structure setting (e.g., in film casting/forming) and achieve improved overall process control.

CRediT authorship contribution statement

Thoithoi Tongbram: Writing – review & editing, Writing – original draft, Visualization, Methodology, Investigation, Funding acquisition, Formal analysis, Data curation, Conceptualization. **Lathika Vaniyan:** Writing – review & editing, Methodology, Investigation, Data curation. **Thomas MacCalman:** Writing – review & editing, Methodology, Data curation. **Avanish Bharati:** Methodology, Investigation. **Frederick J. Warren:** Writing – review & editing, Validation. **Laxmikant Shivnath Badwaik:** Writing – review & editing, Supervision, Project administration. **Pallab Kumar Borah:** Writing – review & editing, Supervision, Methodology, Investigation, Funding acquisition, Formal analysis. **Gleb E. Yakubov:** Writing – review & editing, Supervision, Resources, Project

administration, Methodology, Investigation, Funding acquisition, Formal analysis, Conceptualization.

Declaration of generative AI and AI-assisted technologies in the writing process

Authors have utilised Grammarly AI (GPT 3.5) during the writing of this article to amend grammatical errors and ensure sentence coherence.

Declaration of competing interest

The authors declare that they have no known competing financial interests or personal relationships that could have appeared to influence the work reported in this paper.

Acknowledgement

TT is a Commonwealth Scholar funded by The Commonwealth Scholarship Commission in the UK (INCN-2021-140). GEY acknowledges financial support from Biotechnology and Biological Sciences Research Council (BBSRC Grant No. BB/T006404/1 and BB/W019639/1). TT and GEY acknowledge technical assistance received from Mr Darrell Cobon, Ms Xena Lewis, and Dr Vincenzo Di Bari (School of Biosciences, University of Nottingham, United Kingdom) in performing DSC and turbidity measurements. GEY acknowledges Prof Sushil Dhital, Prof Stephen E. Harding, and Dr Vincenzo Di Bari for many helpful discussions. PKB acknowledges funding received from the European Union's Horizon 2020 research and innovation programme under the Marie Skłodowska-Curie grant agreement No. 101034266 and acknowledges Dr. Seda Ulusoy for useful discussions on XRD. AB acknowledges support from Dr Baohu Wu for assistance on the KWS-X beamline.

Appendix A. Supplementary data

Supplementary data to this article can be found online at https://doi.org/10.1016/j.foodhyd.2025.111936.

Data availability

Data will be made available on request.

References

Ai, Y., & Jane, J.l. (2016). Starch: Structure, property, and determination. In B. Caballero, P. M. Finglas, & F. Toldrá (Eds.), *Encyclopedia of food and health* (pp. 165–174). Academic Press. https://doi.org/10.1016/B978-0-12-384947-2.00657-7.

Allan, M. C., Chamberlain, M., & Mauer, L. J. (2020). Effects of sugars and sugar alcohols on the gelatinization temperatures of wheat, potato, and corn starches. *Foods, 9*(6), 757. https://doi.org/10.3390/foods9060757

Alshammari, N. A., Riches, K., Muttakin, S., Hoad, C. L., Strkalj, L., Gouseti, O., Bakalis, S., Lovegrove, A., Spiller, R. C., Gowland, P. A., Aithal, G. P., Yakubov, G. E., Taylor, M. A., & Marciani, L. (2024). Structuring white rice with gellan gum reduces the glycemic response in healthy humans. *Food Research International, 196*, Article 115090. https://doi.org/10.1016/j.foodres.2024.115090

Baek, M. H., Yoo, B., & Lim, S. T. (2004). Effects of sugars and sugar alcohols on thermal transition and cold stability of corn starch gel. *Food Hydrocolloids, 18*(1), 133–142. https://doi.org/10.1016/S0268-005X(03)00058-4

Balet, S., Guelpa, A., Fox, G., & Manley, M. (2019). Rapid Visco analyser (RVA) as a tool for measuring starch-related physiochemical properties in cereals: A review. *Food Analytical Methods, 12*(10), 2344–2360. https://doi.org/10.1007/s12161-019-01581-w

BeMiller, J. N. (2011). Pasting, paste, and gel properties of starch–hydrocolloid combinations. *Carbohydrate Polymers, 86*(2), 386–423. https://doi.org/10.1016/j.carbpol.2011.05.064

Boehm, M. W., Yakubov, G. E., Delwiche, J. F., Stokes, J. R., & Baier, S. K. (2019). Enabling the rational design of low-fat snack foods: Insights from in vitro oral processing. *Journal of Agricultural and Food Chemistry, 67*(32), 8725–8734. https://doi.org/10.1021/acs.jafc.9b02121

Boehm, M. W., Yakubov, G. E., Stokes, J. R., & Baier, S. K. (2020). The role of saliva in oral processing: Reconsidering the breakdown path paradigm. *Journal of Texture Studies, 51*(1), 67–77. https://doi.org/10.1111/jtxs.12411

Borah, P. K., Deka, S. C., & Duary, R. K. (2017). Effect of repeated cycled crystallization on digestibility and molecular structure of glutinous Bora rice starch. *Food Chemistry, 223*, 31–39. https://doi.org/10.1016/j.foodchem.2016.12.022

Borah, P. K., Rappolt, M., Duary, R. K., & Sarkar, A. (2019a). Effects of folic acid esterification on the hierarchical structure of amylopectin corn starch. *Food Hydrocolloids, 86*, 162–171. https://doi.org/10.1016/j.foodhyd.2018.03.028

Borah, P. K., Rappolt, M., Duary, R. K., & Sarkar, A. (2019b). Structurally induced modulation of in vitro digestibility of amylopectin corn starch upon esterification with folic acid. *International Journal of Biological Macromolecules, 129*, 361–369. https://doi.org/10.1016/j.ijbiomac.2019.02.051

Bouchoux, A., Balmann, H. R.-d., & Lutin, F. (2005). Nanofiltration of glucose and sodium lactate solutions: Variations of retention between single- and mixed-solute solutions. *Journal of Membrane Science, 258*(1), 123–132. https://doi.org/10.1016/j.memsci.2005.03.002

Chakraborty, I., N, P., Mal, S. S., Paul, U. C., Rahman, M. H., & Mazumder, N. (2022). An Insight into the gelatinization properties influencing the modified starches used in food industry: A review. *Food and Bioprocess Technology, 15*(6), 1195–1223. https://doi.org/10.1007/s11947-022-02761-z

Chen, D., Chen, Y., Chen, T., Chen, Y., Xu, Y., Blennow, A., Li, B., & Tian, S. (2025). Effect of tropolone on gray mold rot in harvested fruit and its involved mechanism. *Postharvest Biology and Technology, 219*, Article 113255. https://doi.org/10.1016/j.postharvbio.2024.113255

Chen, Y., Jiang, S., Wang, Y., Zhang, F., Wang, L., Zhao, L., Liu, S., Tan, J., Persson, S., Sun, B., Chen, J., & Blennow, A. (2024). Small-sized starch nanoparticles for efficient penetration of plant cells. *Chemical Communications, 60*(95), 14113–14116. https://doi.org/10.1039/D4CC05493H

Chen, L., Tong, Q., Ren, F., & Zhu, G. (2014). Pasting and rheological properties of rice starch as affected by pullulan. *International Journal of Biological Macromolecules, 66*, 325–331. https://doi.org/10.1016/j.ijbiomac.2014.02.052

Chen, R., Williams, P. A., Shu, J., Luo, S., Chen, J., & Liu, C. (2022). Pectin adsorption onto and penetration into starch granules and the effect on the gelatinization process and rheological properties. *Food Hydrocolloids, 129*, Article 107618. https://doi.org/10.1016/j.foodhyd.2022.107618

Chen, Y., Yang, Q., Xu, X., Qi, L., Dong, Z., Luo, Z., Lu, X., & Peng, X. (2017). Structural changes of waxy and normal maize starches modified by heat moisture treatment and their relationship with starch digestibility. *Carbohydrate Polymers, 177*, 232–240. https://doi.org/10.1016/j.carbpol.2017.08.121

Chen, L., Zhang, H., McClements, D. J., Zhang, Z., Zhang, R., Jin, Z., & Tian, Y. (2019). Effect of dietary fibers on the structure and digestibility of fried potato starch: A comparison of pullulan and pectin. *Carbohydrate Polymers, 215*, 47–57. https://doi.org/10.1016/j.carbpol.2019.03.046

Chun, T., MacCalman, T., Dinu, V., Ottino, S., Phillips-Jones, M. K., & Harding, S. E. (2020). Hydrodynamic compatibility of hyaluronic acid and tamarind seed polysaccharide as ocular mucin supplements. *Polymers, 12*(10), 2272. https://doi.org/10.3390/polym12102272

Ciric, J., Woortman, A. J. J., & Loos, K. (2014). Analysis of isoamylase debranched starches with size exclusion chromatography utilizing PFG columns. *Carbohydrate Polymers, 112*, 458–461. https://doi.org/10.1016/j.carbpol.2014.05.093

Cui, S., Li, M., Zhang, S., Liu, J., Sun, Q., & Xiong, L. (2018). Physicochemical properties of maize and sweet potato starches in the presence of cellulose nanocrystals. *Food Hydrocolloids, 77*, 220–227. https://doi.org/10.1016/j.foodhyd.2017.09.037

Donovan, J. W. (1979). Phase transitions of the starch–water system. *Biopolymers, 18*(2), 263–275. https://doi.org/10.1002/bip.1979.360180204

Durán, E., León, A., Barber, B., & Benedito de Barber, C. (2001). Effect of low molecular weight dextrins on gelatinization and retrogradation of starch. *European Food Research and Technology, 212*(2), 203–207. https://doi.org/10.1007/s002170000205

Fu, Z.-q., Wang, L.-j., Li, D., Zhou, Y.-g., & Adhikari, B. (2013). The effect of partial gelatinization of corn starch on its retrogradation. *Carbohydrate Polymers, 97*(2), 512–517. https://doi.org/10.1016/j.carbpol.2013.04.089

Fu, M., Zhang, Y., Chen, H., Peng, X., & Kan, J. (2025). Effects of three hydrophilic colloids on gelatinization, retrogradation properties, microstructure of highland barley starch and the quality of highland barley noodles. *Food Chemistry, 476*, Article 143424. https://doi.org/10.1016/j.foodchem.2025.143424

Gao, W., Liu, Y., & Wu, S. (2025). Properties of pullulan and its effects on starch gelatinization, retrogradation, and protein interaction: A review. *Food Chemistry, 483*, Article 144337. https://doi.org/10.1016/j.foodchem.2025.144337

Gong, Y., Sui, W., Wang, H., Wang, Y., Li, S., Cui, J., Xie, R., Liu, R., Wu, T., & Zhang, M. (2024). In-depth understanding of the effects of different molecular weight pullulan interacting with protein and starch on dough structure and application properties. *International Journal of Biological Macromolecules, 268*, Article 131556. https://doi.org/10.1016/j.ijbiomac.2024.131556

Hizukuri, S. (1986). Polymodal distribution of the chain lengths of amylopectins, and its significance. *Carbohydrate Research, 147*(2), 342–347. https://doi.org/10.1016/S0008-6215(00)90643-8

Horinaka, J.-i., Okuda, A., Yasuda, R., & Takigawa, T. (2012). Molecular weight between entanglements for linear d-glucans. *Colloid and Polymer Science, 290*(17), 1793–1797. https://doi.org/10.1007/s00396-012-2728-5

Horinaka, J.-i., Yasuda, R., & Takigawa, T. (2011). Entanglement properties of cellulose and amylose in an ionic liquid. *Journal of Polymer Science Part B: Polymer Physics, 49*(13), 961–965. https://doi.org/10.1002/polb.22262

Hsieh, C.-F., Liu, W., Whaley, J. K., & Shi, Y.-C. (2019). Structure and functional properties of waxy starches. *Food Hydrocolloids, 94*, 238–254. https://doi.org/10.1016/j.foodhyd.2019.03.026

Jenkins, P. J., & Donald, A. M. (1998). Gelatinisation of starch: A combined SAXS/WAXS/DSC and SANS study. *Carbohydrate Research, 308*(1), 133–147. https://doi.org/10.1016/S0008-6215(98)00079-2

Junejo, S. A., Flanagan, B. M., Zhang, B., & Dhital, S. (2022). Starch structure and nutritional functionality – Past revelations and future prospects. *Carbohydrate Polymers, 277*, Article 118837. https://doi.org/10.1016/j.carbpol.2021.118837

Jung, D.-H., Park, C.-S., Kim, H.-S., Nam, T. G., Lee, B.-H., Baik, M.-Y., Yoo, S.-H., & Seo, D.-H. (2022). Enzymatic modification of potato starch by amylosucrase according to reaction temperature: Effect of branch-chain length on structural, physicochemical, and digestive properties. *Food Hydrocolloids, 122*, Article 107086. https://doi.org/10.1016/j.foodhyd.2021.107086

Kew, B., Holmes, M., Stieger, M., & Sarkar, A. (2021). Oral tribology, adsorption and rheology of alternative food proteins. *Food Hydrocolloids, 116*, Article 106636. https://doi.org/10.1016/j.foodhyd.2021.106636

Khin, M. N. O. E., Ahammed, S., & Zhong, F. (2021). Development of (5-(4,6-dichlorotriazinyl) aminofluorescein) DTAF-labelled polysaccharides for characterization of microstructure and phase distribution of composite hydrogel visualization of hydrogels using CLSM. *Food Bioscience, 41*, Article 100909. https://doi.org/10.1016/j.fbio.2021.100909

Kohyama, K., & Nishinari, K. (1991). Effect of soluble sugars on gelatinization and retrogradation of sweet potato starch. *Journal of Agricultural and Food Chemistry, 39*(8), 1406–1410. https://doi.org/10.1021/jf00008a010

Krystyjan, M., Dobosz-Kobędza, A., Sikora, M., & Baranowska, H. M. (2022). Influence of Xanthan Gum addition on the Short- and long-term retrogradation of corn starches of various amylose content. *Polymers, 14*(3), 452. https://doi.org/10.3390/polym14030452

Kühner, F., Erdmann, M., & Gaub, H. E. (2006). Scaling exponent and Kuhn Length of pinned polymers by single molecule force spectroscopy. *Physical Review Letters, 97*(21), Article 218301. https://doi.org/10.1103/PhysRevLett.97.218301

Le-Bail, P., Hesso, N., & Le-Bail, A. (2018). Chapter 15 - Starch in baked products. In M. Sjöö, & L. Nilsson (Eds.), *Starch in food* (2nd ed., pp. 595–632). Woodhead Publishing. https://doi.org/10.1016/B978-0-08-100868-3.00015-9.

Li, C., Dhital, S., Gilbert, R. G., & Gidley, M. J. (2020). High-amylose wheat starch: Structural basis for water absorption and pasting properties. *Carbohydrate Polymers, 245*, Article 116557. https://doi.org/10.1016/j.carbpol.2020.116557

Li, C., & Hu, Y. (2021). Effects of acid hydrolysis on the evolution of starch fine molecular structures and gelatinization properties. *Food Chemistry, 353*, Article 129449. https://doi.org/10.1016/j.foodchem.2021.129449

Li, C., Ji, Y., Zhang, S., Yang, X., Gilbert, R. G., Li, S., & Li, E. (2022). Amylose inter-chain entanglement and inter-chain overlap impact rice quality. *Foods, 11*(10). https://doi.org/10.3390/foods11101516

Li, Q., Li, H., & Gao, Q. (2015). The influence of different sugars on corn starch gelatinization process with digital image analysis method. *Food Hydrocolloids, 43*, 803–811. https://doi.org/10.1016/j.foodhyd.2014.08.012

Luo, D., Li, Y., Xu, B., Ren, G., Li, P., Li, X., Han, S., & Liu, J. (2017). Effects of inulin with different degree of polymerization on gelatinization and retrogradation of wheat starch. *Food Chemistry, 229*, 35–43. https://doi.org/10.1016/j.foodchem.2017.02.058

Ma, S., Zhu, P., & Wang, M. (2019). Effects of konjac glucomannan on pasting and rheological properties of corn starch. *Food Hydrocolloids, 89*, 234–240. https://doi.org/10.1016/j.foodhyd.2018.10.045

Mao, Y., Shi, J., Cai, L., Hwang, W., & Shi, Y.-C. (2023). Microstructures of starch granules with different amylose contents and Allomorphs as revealed by scattering techniques. *Biomacromolecules, 24*(5), 1980–1993. https://doi.org/10.1021/acs.biomac.2c01240

Osmanović, D. (2018). Properties of Rouse polymers with actively driven regions. *The Journal of Chemical Physics, 149*(16), Article 164911. https://doi.org/10.1063/1.5045686

Pérez, S., & Bertoft, E. (2010). The molecular structures of starch components and their contribution to the architecture of starch granules: A comprehensive review. *Starch - Stärke, 62*(8), 389–420. https://doi.org/10.1002/star.201000013

Perry, P. A., & Donald, A. M. (2002). The effect of sugars on the gelatinisation of starch. *Carbohydrate Polymers, 49*(2), 155–165. https://doi.org/10.1016/S0144-8617(01)00324-1

Popov, D., Buléon, A., Burghammer, M., Chanzy, H., Montesanti, N., Putaux, J. L., Potocki-Véronèse, G., & Riekel, C. (2009). Crystal structure of A-amylose: A revisit from synchrotron microdiffraction analysis of single crystals. *Macromolecules, 42*(4), 1167–1174. https://doi.org/10.1021/ma801789j

Pourmohammadi, K., Abedi, E., Hashemi, S. M. B., & Torri, L. (2018). Effects of sucrose, isomalt and maltodextrin on microstructural, thermal, pasting and textural properties of wheat and cassava starch gel. *International Journal of Biological Macromolecules, 120*, 1935–1943. https://doi.org/10.1016/j.ijbiomac.2018.09.172

Ratnayake, W. S., & Jackson, D. S. (2007). A new insight into the gelatinization process of native starches. *Carbohydrate Polymers, 67*(4), 511–529. https://doi.org/10.1016/j.carbpol.2006.06.025

Ren, Y., Yakubov, G. E., Linter, B. R., & Foster, T. J. (2021). Development of a separated-dough method and flour/starch replacement in gluten free crackers by cellulose and fibrillated cellulose. *Food & Function, 12*(18), 8425–8439. https://doi.org/10.1039/D1FO01368H

Renzetti, S., van den Hoek, I. A. F., & van der Sman, R. G. M. (2021). Mechanisms controlling wheat starch gelatinization and pasting behaviour in presence of sugars and sugar replacers: Role of hydrogen bonding and plasticizer molar volume. *Food Hydrocolloids, 119*, Article 106880. https://doi.org/10.1016/j.foodhyd.2021.106880

Sarko, A., & Biloski, A. (1980). Crystal structure of the koh-amylose complex. *Carbohydrate Research, 79*(1), 11–21. https://doi.org/10.1016/S0008-6215(00)85127-7

Sheng, L., Li, P., Wu, H., Liu, Y., Han, K., Gouda, M., Tong, Q., Ma, M., & Jin, Y. (2018). Tapioca starch-pullulan interaction during gelation and retrogradation. *Lebensmittel-Wissenschaft und -Technologie, 96*, 432–438. https://doi.org/10.1016/j.lwt.2018.05.064

Shi, J., Sweedman, M. C., & Shi, Y.-C. (2021). Structure, birefringence and digestibility of spherulites produced from debranched waxy maize starch. *International Journal of Biological Macromolecules, 183*, 1486–1494. https://doi.org/10.1016/j.ijbiomac.2021.05.127

Vaniyan, L., Borah, P. K., Pavlovskaya, G. E., Terrill, N., Reid, J. E. S. J., Boehm, M., Prochasson, P., Nicholson, R. A., Baier, S., & Yakubov, G. E. (2025). Wet spinning of sodium carboxymethyl cellulose–sodium caseinate hydrogel fibres: Relationship between rheology and spinnability. *Soft Matter, 21*, 3946–3956. https://doi.org/10.1039/D4SM00705K

Waigh, T. A., Gidley, M. J., Komanshek, B. U., & Donald, A. M. (2000). The phase transformations in starch during gelatinisation: A liquid crystalline approach. *Carbohydrate Research, 328*(2), 165–176. https://doi.org/10.1016/S0008-6215(00)00098-7

Waigh, T. A., Perry, P., Riekel, C., Gidley, M. J., & Donald, A. M. (1998). Chiral side-chain liquid-crystalline polymeric properties of starch. *Macromolecules, 31*(22), 7980–7984. https://doi.org/10.1021/ma971859c

Wang, S., Li, C., Copeland, L., Niu, Q., & Wang, S. (2015). Starch retrogradation: A comprehensive review. *Comprehensive Reviews in Food Science and Food Safety, 14*(5), 568–585. https://doi.org/10.1111/1541-4337.12143

Wang, L., Xu, J., Fan, X., Wang, Q., Wang, P., Yuan, J., Yu, Y., Zhang, Y., & Cui, L. (2018). The effect of branched limit dextrin on corn and waxy corn gelatinization and retrogradation. *International Journal of Biological Macromolecules, 106*, 116–122. https://doi.org/10.1016/j.ijbiomac.2017.07.181

Wang, L., Xu, J., Fan, X., Wang, Q., Wang, P., Zhang, Y., Cui, L., Yuan, J., & Yu, Y. (2016). Effect of disaccharides of different composition and linkage on corn and waxy corn starch retrogradation. *Food Hydrocolloids, 61*, 531–536. https://doi.org/10.1016/j.foodhyd.2016.06.010

Wang, S., Zhang, X., Wang, S., & Copeland, L. (2016). Changes of multi-scale structure during mimicked DSC heating reveal the nature of starch gelatinization. *Scientific Reports, 6*(1), Article 28271. https://doi.org/10.1038/srep28271

Whelan, W. J. (1971). Enzymic explorations of the structures of starch and glycogen. *Biochemical Journal, 122*(5), 609–622. https://doi.org/10.1042/bj1220609

Xu, L., Ren, J., Wang, X., Bai, Z., Chai, S., & Wang, X. (2023). Effects of sugar beet pectin on the pasting, rheological, thermal, and microstructural properties of wheat starch. *International Journal of Biological Macromolecules, 253*, Article 127328. https://doi.org/10.1016/j.ijbiomac.2023.127328

Yakubov, G. E., Zhong, L., Li, M., Boehm, M. W., Xie, F., Beattie, D. A., Halley, P. J., & Stokes, J. R. (2015). Lubrication of starch in ionic liquid–water mixtures: Soluble carbohydrate polymers form a boundary film on hydrophobic surfaces. *Carbohydrate Polymers, 133*, 507–516. https://doi.org/10.1016/j.carbpol.2015.06.087

Yang, Z., Swedlund, P., Hemar, Y., Mo, G., Wei, Y., Li, Z., & Wu, Z. (2016). Effect of high hydrostatic pressure on the supramolecular structure of corn starch with different amylose contents. *International Journal of Biological Macromolecules, 85*, 604–614. https://doi.org/10.1016/j.ijbiomac.2016.01.018

Ye, Y., Liao, L., Yang, R., Zhang, S., Zhang, J., Zhang, J., Wu, W., & Zhang, Y. (2024). Inhibitory effect of different degree of polymerization inulin on the retrogradation of rice starch gels and fresh rice noodles. *Lebensmittel-Wissenschaft und -Technologie, 213*, Article 117001. https://doi.org/10.1016/j.lwt.2024.117001

Zhan, Y., Dai, H., Ma, L., & Zhang, Y. (2025). Gelatinization, rheological and retrogradation behaviors of waxy rice starch affected by gelatin emulsion and regulation mechanism. *Food Hydrocolloids, 159*, Article 110649. https://doi.org/10.1016/j.foodhyd.2024.110649

Zhang, Y., Li, G., Wu, Y., Yang, Z., & Ouyang, J. (2019). Influence of amylose on the pasting and gel texture properties of chestnut starch during thermal processing. *Food Chemistry, 294*, 378–383. https://doi.org/10.1016/j.foodchem.2019.05.070

Zhao, Y., Wang, J., He, R., Ren, Y., Fu, J., Zeng, Y., Zhang, K., & Zhong, G. (2024). Integrative experimental and computational analysis of the impact of KGM's polymerization degree on wheat starch's pasting and retrogradation characteristics. *Carbohydrate Polymers, 346*, Article 122570. https://doi.org/10.1016/j.carbpol.2024.122570

Zhou, D.-N., Zhang, B., Chen, B., & Chen, H.-Q. (2017). Effects of oligosaccharides on pasting, thermal and rheological properties of sweet potato starch. *Food Chemistry, 230*, 516–523. https://doi.org/10.1016/j.foodchem.2017.03.088